NTNU
Norwegian University of Science and Technology

The Norwegian University of Science and Technology

Norges Teknisk-Naturvitenskapelige Universitet

ADDRESS:
NTNU

DEPARTMENT OF ENERGY AND PROCESS Engineering

Kolbjørn Hejes vei 1A, N-7491 Trondheim - NTNU

TELEPHONE
Switchboard NTNU: 73 59 40 00
Department office: 73 59 27 00
Hydropower section: 73 59 38 57

TELEFAX
Department office: 73 59 83 90
Hydropower section: 73 59 38 54

Report no:
EPT-M-2009-87

Classification:

Title of report

Heat- and mass transfer in ammonia-water absorption systems

Author

Andreas Heufken

Date 09.02.2010

No. of pages/appendices 75

Project manager

Prof. Eikevik

Division

Faculty of Engineering Science and technology

Department of Energy and Process Engineering

Project no.

ISBN no.

Price group

Client/Sponsor of project

Client's ref.

Abstract

A literature review of experimental investigations for ammonia-water absorbers systems in the last 30 years and a test facility was designed to measure heat and mass transfer. It is well known that the absorber within an absorption system is the "bottleneck" in terms of size, costs and efficiency. The research in the common absorber design of horizontal and vertical falling film absorbers focused on improving the desired disadvantages of coolant heat transfer, wetability problems with weak solution distribution and increasing surface area between ammonia vapor and solution. Several absorber designs have been developed and this thesis gives an overview of investigations and their results. A bubble absorber where ammonia vapor bubbles into weak solution was extensively investigated and researchers designated bubble absorber as the best possible design for ammonia-water absorbers. Accordingly the idea of adding surfactants and nano particles to enhance mass and heat transfer was extensively investigated mainly by Kang. The addition showed promising possibilities but no results for long term usage were found.

From the wide range of investigations a test facility was designed to measure heat and mass transfer in ammonia-water absorption system. The decision was made to build a test facility for bubble absorption to experimentally verify a numerical model which will be investigated in a further PhD thesis. The test section was designed variable in terms of inner diameter to find an optimum inner diameter and also compare results to plate heat exchangers with small inner diameter. The test section can also be reconstructed to a transparent system to focus on bubble flow pattern and influence of nozzle and orifice of bubble disappearance.

	Indexing Terms: English	Norwegian
Group 1	absorption, ammonia-water	
Group 2	heat and mass transfer	
Selected by author	Absorber, experimental	

Norwegian University of Science and Technology

Faculty of Engineering Science and Technology

Heat- and mass transfer in ammonia-water absorption systems

Varme og massetransport i apsorpsjonskretser med ammoniak/vann

Department of Energy and Process Engineering

Prof. Trygve M. Eikevik

Tom S. Nordtvedt

Andreas Heufken

Trondheim

February 9, 2010

Abstract

A literature review of experimental investigations for ammonia-water absorbers systems in the last 30 years and a test facility was designed to measure heat and mass transfer. It is well known that the absorber within an absorption system is the “bottleneck” in terms of size, costs and efficiency. The research in the common absorber design of horizontal and vertical falling film absorbers focused on improving the desired disadvantages of coolant heat transfer, wetability problems with weak solution distribution and increasing surface area between ammonia vapor and solution. Several absorber designs have been developed and this thesis gives an overview of investigations and their results. Another approach in solving the task was a new absorber design mainly introduced by Ferreira. A bubble absorber where ammonia vapor bubbles into weak solution was extensively investigated and researchers designated bubble absorber as the best possible design for ammonia-water absorbers. Accordingly the idea of adding surfactants and nano particles to enhance mass and heat transfer was extensively investigated mainly by Kang. The addition showed promising possibilities but no results for long term usage were found.

From the wide range of investigations a test facility was designed to measure heat and mass transfer in ammonia-water absorption system. The decision was made to build a test facility for bubble absorption to experimentally verify a numerical model which will be investigated in a further PhD thesis. The test section was designed variable in terms of inner diameter to find an optimum inner diameter and also compare results to plate heat exchangers with small inner diameter. The test section can also be reconstructed to a transparent system to focus on bubble flow pattern and influence of nozzle and orifice of bubble disappearance.

Abstract

Eine Literatur Recherche über die experimentellen Untersuchungen der letzten 30 Jahre in Bezug auf Ammoniak-Wasser Absorber wurde erstellt. Zusätzlich wurde ein Teststand entwickelt, um Wärme- und Stoffübertragung innerhalb eines Absorbers zu messen. Der Absorber in einer Absorptionsmaschine ist bekannt als „Flaschenhals“ innerhalb des Systems bezüglich Größe, Kosten und Effektivität. Die Untersuchungen von Rieselfilmabsorbern, die am weitesten verbreitet sind, konzentrierten sich in erster Linie darauf, die Probleme innerhalb des Absorbers zu lösen oder zu minimieren. Zu diesen Nachteilen zählen Kühlmittelwärmeübertragung, gleichmäßige Oberflächenbenetzung mit Ammoniak-Lösung und eine Erhöhung der Oberfläche zwischen Ammoniak-Lösung und Ammoniakdampf. Ein anderer Ansatz, um die Effektivität zu verbessern, ist die Entwicklung eines neuartigen Absorber Designs. Ferreira war einer der ersten, der einen Blasenabsorber getestet hat, in dem Ammoniakdampf in ein vertikales Rohr blubbert und absorbiert wird. Im Anschluss wurde dieses Design intensiv erforscht und man kam zu dem Schluss, dass Blasenabsorber die beste Performance für ein Ammoniak-Wasser System darstellen. Weiterhin wurde besonders von Kang die Möglichkeit untersucht Tenside und Nano-Partikel der Ammoniak-Losung hinzuzufügen, um die Wärme- und Stoffübertragung zu verbessern. Die vorgestellten Ergebnisse sind erfolgsversprechend, allerdings fehlen Langzeittests und Untersuchungen die das gesamte Absorptionssystem betrachten.

Aus der großen Vielfalt an Testständen und Möglichkeiten die gewünschten Parameter zu erreichen und zu messen, wurde ein Blasenabsorber gewählt. Der teststand konzentriert sich darauf in großem Umfang Temperaturen, Druck, Konzentrationen, Durchmesser und Massenströme zu variieren und deren Einfluss auf die Wärme- und Stoffübertragung zu messen. Im Anschluss an die experimentellen Untersuchungen wird eine Doktorarbeit geschrieben, um die experimentellen Ergebnisse in einem numerischen Modell nachzustellen. Der Teststand kann aber ebenso durch Austausch der Edelstahlrohre durch Plexi-Glas umgebaut werden, um die Entstehung der Blasen und deren Flussmodell visuell zu untersuchen. Der anfängliche turbulente Bereich der Blasenentstehung ist der Bereich mit dem größten Wärme- und Stofftransport und Möglichkeiten diesen zu erhöhen könnten untersucht werden.

Table of Contents

Nomenclature

A	surface area
c	specific heat capacity
d	diameter
g	gravity
h	enthalpy
H	overall mass transfer coefficient
$\dot{m}$	mass flow rate
p	pressure
$\dot{q}$	heat transfer rate
T	temperature
s	entropy
s	thickness
U	overall heat transfer coefficient
V	volume
x	mass concentration

Greek

ρ	density
ξ	molar concentration
μ	viscosity
σ	tension

Subscripts

c	coolant
i	inlet
l	liquid
m	mean
o	outlet
p	pressure
rs	rich solution
ss	strong solution
v	vapor
ws	weak solution

1 Introduction

This chapter gives an overview about the history of refrigeration and the possible new fields for absorption cycles. The two dominating refrigeration cycles vapor compression and vapor absorption are briefly explained and the two typical working pairs for an absorption refrigeration system are depicted.

1.1 History

Vapor absorption refrigeration cycles have existed for decades. Ammonia-water has been used as a working pair in absorption refrigeration systems since 1846 when Ferdinand Carré built the first successful machine and registered his machine in 1859 under a British patent. Ammonia-water absorption refrigerators were widely used in the middle of the 20th century and they have been drawing a renewed attention with the growing awareness of global warming and ozone depletion due to the fact that ammonia has zero global warming potential (GWP), ozone depletion potential (ODP) and is heat driven by low grade heat. Therefore it has the potential to save electricity used in conventional compressor refrigerators and use waste heat or solar heat.

1.2 Refrigeration Cycles

Refrigeration is the remove of heat at a temperature below ambient. This is according to the second law of thermodynamics only possible when the heat is pumped to a higher temperature level over ambient by mechanical (vapor compression cycle) or thermal (vapor absorption cycle) energy.

The heat is removed by evaporating the refrigerant at a low pressure level and is rejected afterwards by condensation on a high pressure level to the ambient.

1.3 Vapor compression cycle

In vapor compression cycles cold is produced by electrical energy (a_{t12}) which drives the compressor to compress the refrigerant to a higher pressure level. After the compression (1->2) the refrigerant is cooled and condensed in the condenser (2->4). Thereafter it is decompressed by an expansion valve into the evaporator (4->5) to gain the heat duty (5->1). The extraction of heat at this low temperature level is called the production of cold. The steps within this cycle are depicted in a t-s-diagram xx.

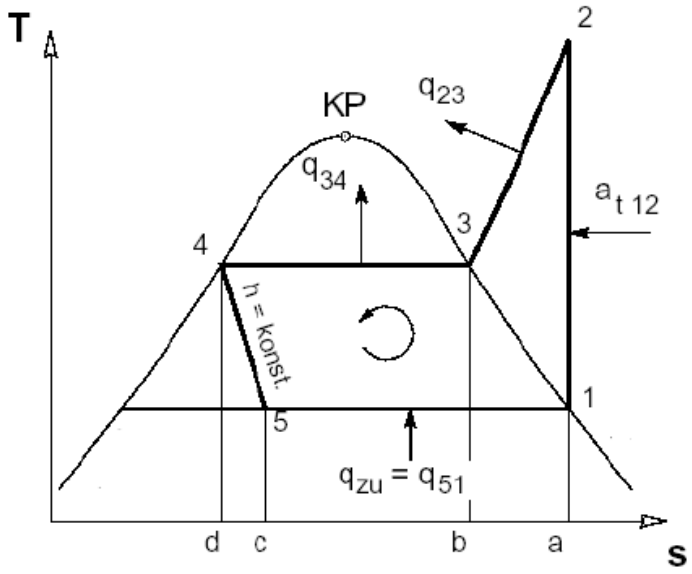

Figure 1.1: T-s-diagram of vapor compression cycle

1.4 Vapor absorption cycle

The vapor absorption cycle is the same as vapor compression cycle except the compressor. The compressor is replaced by an absorber, pump, generator and an expansion valve. The refrigerant is replaced by a working pair labeled as the absorbent and the refrigerant.

In the absorber (A) the refrigerant is absorbed by the absorbent. The heat of absorption has to be removed (Q_{ab}) to ensure the progress since the absorption potential is a function of temperature, pressure and concentration. Afterwards the rich solution is pumped (P) to the generator (AT) to a higher pressure level where the refrigerant evaporates driven by a heat source (Q_{heiz}). The refrigerant condensates like in the vapor compression cycle in the condenser (Ko), expanded (Dr) and evaporated in the evaporator (V). The weak solution on the other hand is expanded by an expansion valve (LD) to the absorber to absorb the refrigerant. In common vapor absorption machines a solution heat exchanger (WT) is included to preheat the rich solution and precool the weak solution.

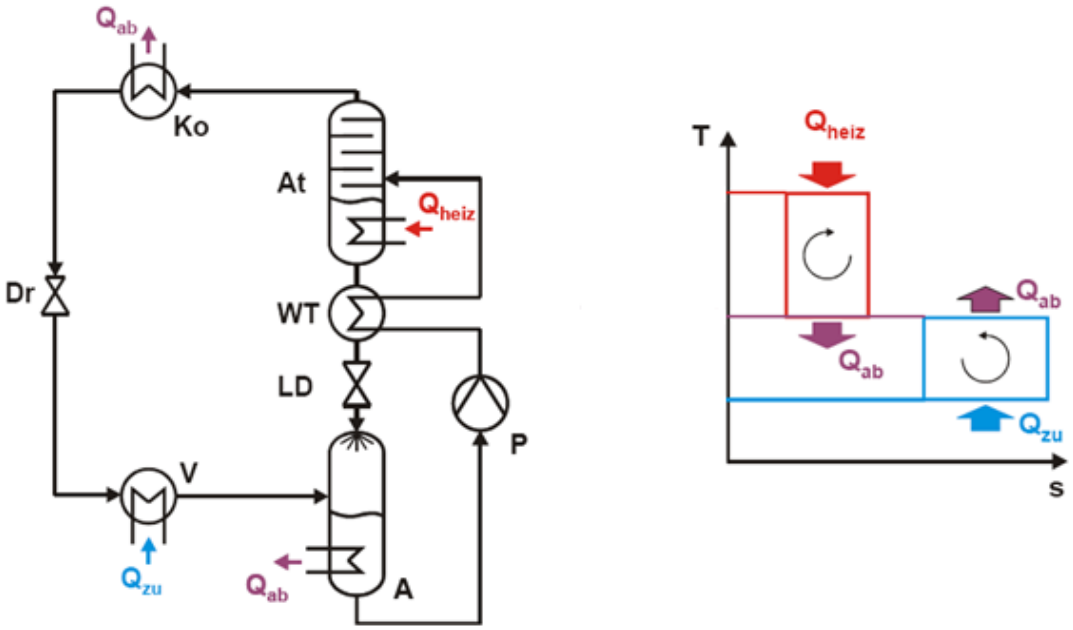

Figure 1.2: Schematic diagram and t-s-diagram of an absorption cooling cycle [45]

1.5 Working pairs for vapor absorption cycles

Ammonia-water and LiBr-water are the common pairs used in absorption refrigeration cycles, where ammonia is the refrigerant and water the absorbent and water is the refrigerant and a weak solution of LiBr-water is the absorber in the other pair. Therefore the ammonia system has the potential to produce temperatures under 0C but needs an additional rectifier due to the fact that water is a volatile absorber.

This study focuses on ammonia-water absorption cycles and predictions are assumed to be made only for this system.

1.6 Absorber

The absorber has the purpose to absorb the refrigerant´s vapor into the weak solution and to distribute the heat of absorption to a coolant.

The driving force of this task is the difference between weak solution concentration and saturation at a given temperature and pressure. During the absorption the weak solution enriches, the temperature rises because of the exothermal absorption and the driving force decreases. Therefore the heat must be distributed to the coolant to obtain high mass transfer. The absorption takes place in a small area between the bulk vapor and solution. The design of the absorber has the purpose to deliver the heat of absorption through the absorption area over the bulk weak solution to the coolant. Therefore good heat transfer within the liquid and to the coolant is important.

This coupled heat and mass transfer is the task which has to be improved with the absorber design in order to build small and efficient absorber.

1.7 Classification of Absorber

The history of absorber designs as mentioned by Niebergall [43] started with dualpipe absorbers until 30th of last century with coolant in the inner tube and gas/weak solution in outer tube mixing and absorbing. Problems occurred with different cooling loads. An improvement is the multipipe absorber with at least seven pipes. Several cooling water pipes are surrounded by pipes of gas-weak solution and the gas is injected at different locations into the outer pipe bubbling into the liquid. This results in increased mass transfer and decreased pressure losses.

In coolant spray absorbers the cooling water sprinkles over pipes of weak solution and gas is injected on different locations into the pipes.

Horizontal and vertical shell and tubular absorbers consist of cooling water in the pipes and weak solution and ammonia gas flows around the pipes forced by baffles.

In horizontal and vertical falling film absorbers the vessel is filled with gas and cooling water flows through pipes. The weak solution enters the absorber by a distributor to ensure a high wet ability of the horizontal coolant tubes. Ammonia vapor is sucked out of the evaporator

and the enriched solution leaves the absorber at the bottom. This design has a low solution amount and vertical design decreases amount of building area. However the wet ability is a problem.

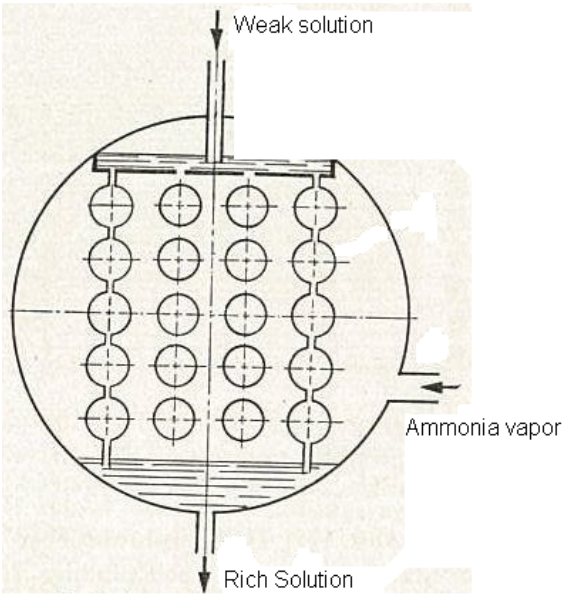

Figure 1.3: Falling film absorber [43]

Vertical tubular bubble absorbers are a compromising design for ammonia-water refrigeration cycles. The vapor is bubbled into the weak solution in vertical tubes and the coolant surrounds the pipes in a dualpipe design. The coolant and weak solution can either be in co or counter current flow. The bubble flow can be divided into 3 flows. First at the entrance there is a churn flow with high mass transfer coefficients. After that a long part of well shaped tailor bubbles with a thin film between the pipe and the bubble. The tailor bubbles also provide good mass transfer and furthermore good heat transfer due to the small amount of solution surrounding the bubbles. This is accounted to the small amount of bulk solution where the heat of mass transfer must be transported out of the thin film. The last flow pattern is rising bubbles decreasing to full absorption.

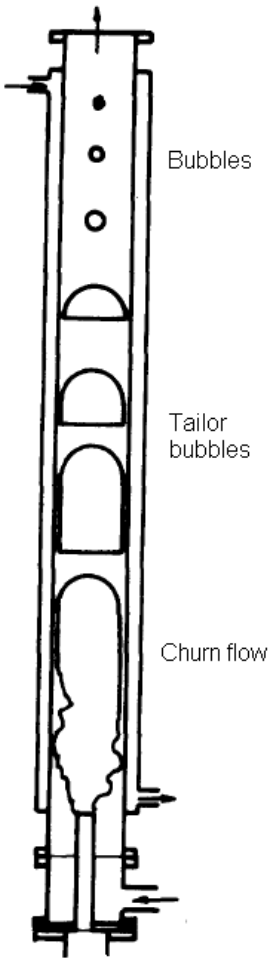

Figure 1.4: Bubble flow pattern [9]

1.8 GAX cycle

The GAX-cycle is an improved vapor absorption cycle with an additional generator absorber heat exchanger first introduced by Altenkirch [1]. The heat of absorption in the absorber is transferred to the rich solution in the generator to produce ammonia vapor. Therefore the necessary heat from steam or other heat sources to produce ammonia vapor is decreased as depicted in Figure 1.5. The disadvantage of this cycle is the additional heat exchanger and the low solution flow to obtain a temperature overlap of the absorber and generator to produce vapor. The wetability problems in common falling film absorbers especially for low solution flow prevents the GAX-cycle development. Therefore the purpose of some investigations described later is to solve the wetability problem for low solution flow or design new absorbers i.e. bubble absorbers to prohibit this disadvantage.

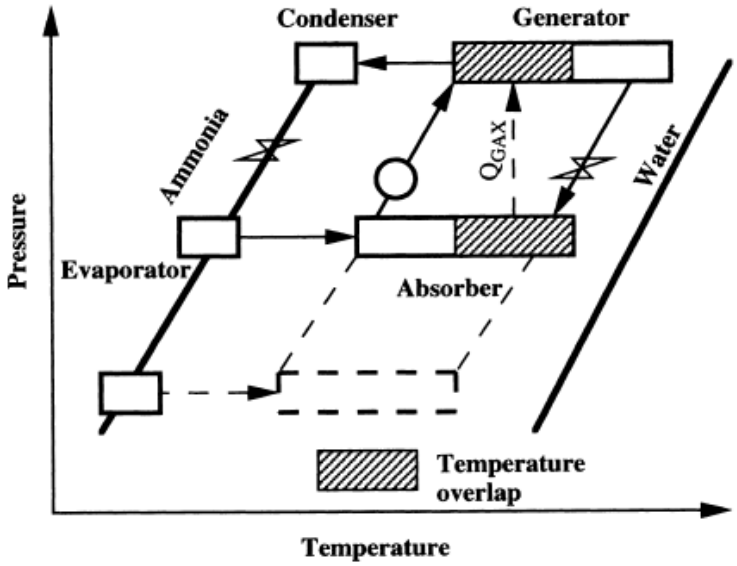

Figure 1.5: p-t-diagram of a GAX-cycle

1.9 Dimensionless numbers

Dimensionless numbers are often used to describe processes in heat and mass transfer. They provide the possibility to adopt mechanisms from a model to a more complex process. Initiated by Reynolds in 1883 by his similarity law, which said that flows from a simple model can be adopted for the original when the Reynolds numbers are similar, a lot of dimensionless numbers were introduced. An overview of the numbers used is the purpose of this chapter.

Reynolds number: $$\mathrm{Re}_v = \frac{\rho_v V_0 d_0}{\mu_v} = \frac{inertial\ force}{viscous\ force}$$

Nusselt number: $$Nu = \frac{hL}{k_f} = \frac{convective\,heat\,transfer\,coefficient}{conductive\,heat\,transfer\,coefficient}$$

Schmidt number: $$Sc = \frac{\mu}{\rho D} = \frac{viscous\,diffusion\,rate}{molecular\,diffusion\,rate}$$

Sherwood number: $$Sh = \frac{K \cdot L}{D} = \frac{convective\,mass\,transfer\,coefficient}{diffusive\,mass\,transfer\,coefficient}$$

Weber number: $$We_v = \frac{V_0^2 d_0 \rho_v}{\sigma} = \frac{inertial\ force}{surface\,tension\ force}$$

Buoyancy number: $$Bu_v = \frac{V_0^2 \rho_v}{g d_0 \Delta\rho} = \frac{inertial\ force}{buoyancy}$$

Froud number: $$Fr = \frac{v}{\sqrt{gD}} = \frac{inertial\ force}{gravital\ force}$$

Galileo number: $$Ga_v = \frac{g\rho_1(\rho_1 - \rho_v)d_v^3}{\mu_1^2} = \frac{buoyancy\ force}{viscous\ force}$$

1.10 Motivation

Although the absorber is acknowledged as the most important part and labeled as the "bottleneck" in terms of efficiency, costs and size, accurate model equations for designing an absorber have not been available yet.

A lot of research can be found for LiBr-water but not for ammonia-water due to the fact that the volatile absorbent makes it difficult to establish an exact model.

The research about different ammonia-water absorbers of the last decades has found some compromising designs but no innovation has been included in the commercial market.

The motivation of this study is to determine the different improvements by designing new absorbers and to find a compromising absorber. After that developing a test rig to investigate the absorber design in a basic single pipe model and find the best parameters to obtain a small scale absorber.

2 Literature review

This chapter gives an overview of the research in the last decades about absorber designs numerical and analytical. The chapter is classified by the two major absorber designs thin film absorption and bubble absorption additional the chapters surfactants and nano particles are added as a possible improvement for absorption systems. The review only includes absorption research in the field of ammonia-water absorption although some conclusions of LiBr-water absorption and general absorption investigations can be found and adopted.

2.1 Falling Film Absorption

Falling film absorbers with horizontal and vertical coolant tubes have been widely utilized in commercial absorption systems. This design provides low pressure drop on the vapor side but also has a low heat transfer area and an unstable liquid distribution. Various mass and heat transfer enhancement techniques such as surface profiling, extended fins, miniaturization and use of surfactants have been extensively investigated by researchers. A comprehensive overview of analytical investigations for volatile and nonvolatile absorbents for falling film absorption can be found at Killion and Garimella [27]. Only a few papers, however, have been found on the experimental analysis.

2.1.1 Experimental work

Kang et al. [19] investigated the coupled heat and mass transfer and focused on the influence of subcooling of the weak solution. He used a half closed cycle to investigate a plate heat exchanger with offset strip fins (OSF) for the solution side and rectangular fins for the coolant side as depicted in Figure 2.1. The purpose of OSF was the enhanced mixing while flowing down from fin to fin.

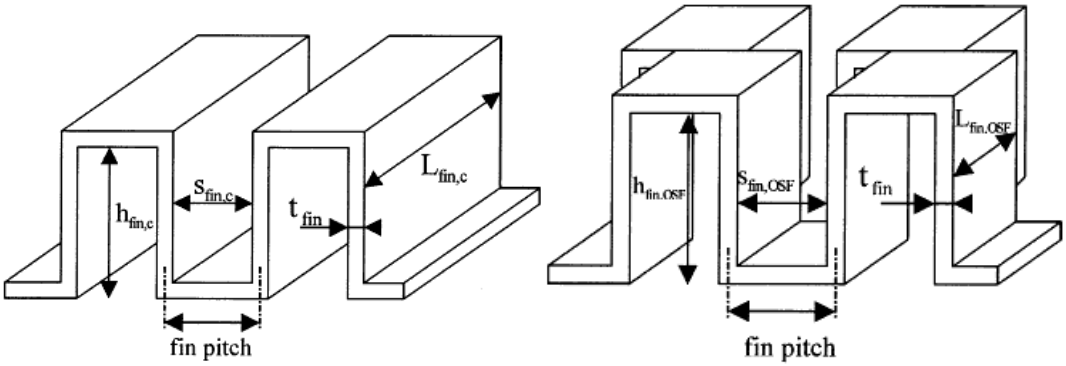

Figure 2.1: Rectangular plain fin and offset strip fin [19]

Figure 2.2 depicts the half closed cycle consisting of a vapor production cycle, a solution distribution cycle, a coolant cycle and a rich solution cycle for neutralization. The 20% ammonia-water solution is heated and therefore vapor is produced for injection into the test section. The vapor has an ammonia concentration of 65% to 80% and the weak solution concentration ranges from 5% to 15%. The solution enters the test section co current to the vapor at the top of the test section flows cross-counter current to the coolant and leaves the test section at the bottom.

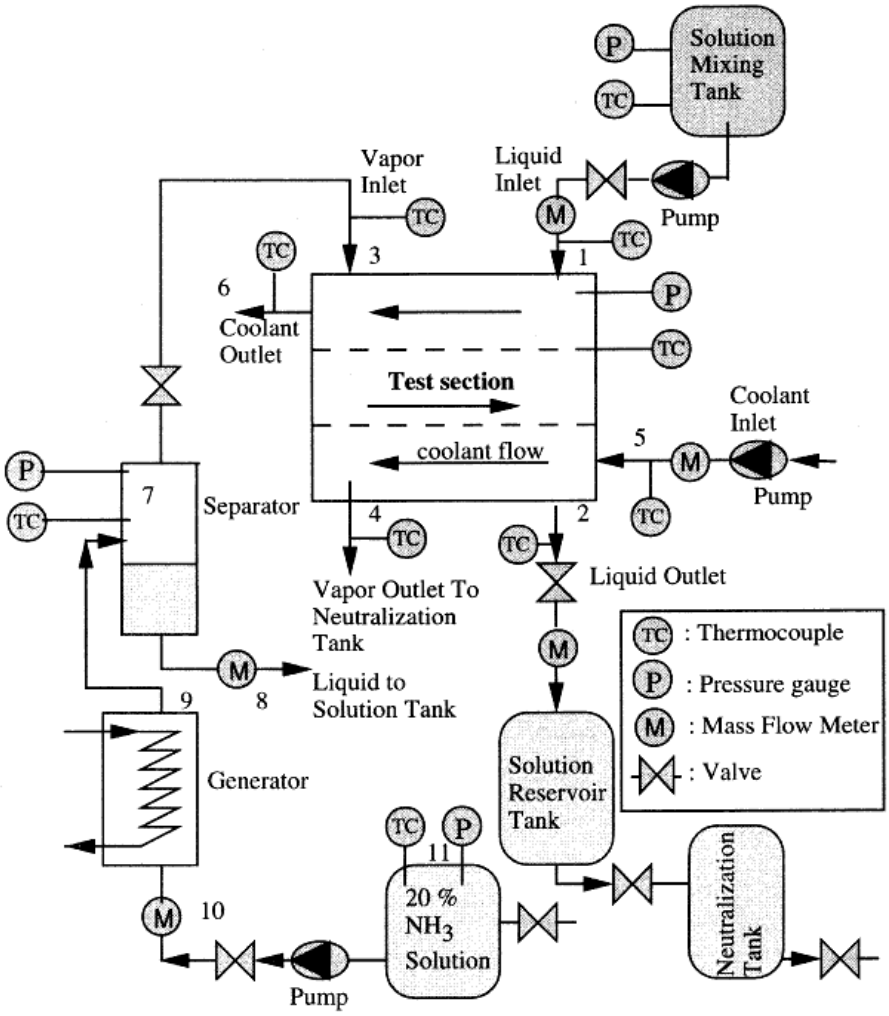

Figure 2.2: Schematic diagram of the apparatus [19]

Water rectification occurs at the top of the test section due to the subcooling of weak solution. After the rectification process, the bulk vapor concentration becomes higher than the equilibrium vapor concentration, thereafter the absorption starts. Kang concluded that the subcooling of the weak solution has a more significant effect on the heat transfer than mass transfer. Increasing the concentration difference increases mass flow and decreases heat transfer. The heat and mass transfer coefficients ranged 500 - 2100 W/m²K and $1.0 - 55 \cdot 10^{-8}$ m/s, respectively.

From the parametric analysis based on the experimental data Kang inferred that increasing the liquid flow rate which results in increasing liquid Reynolds number has a more significant effect on heat transfer and increasing vapor flow rate and therefore increasing Vapor Reynolds number has a more significant effect on mass transfer. Hence he concluded that

the mass transfer resistance is dominant in the vapor phase and heat transfer resistance is dominant in the liquid phase.

Regarding the simple separator the vapor has an ammonia concentration of 65% to 80% which is not a typical condition in absorption systems. The rectification is caused by low ammonia concentrations and the effort to produce quite pure ammonia vapor should be considered. Rectification decreases the heat load of the absorber and therefore distorts the results.

Kwon and Jeong [34] investigated a helical coil thin film absorber as depicted in Figure 2.3. The weak solution drips from 16 nozzles with a diameter of 2mm. Vapor can be introduced at the top and bottom to obtain parallel or counter current flow.

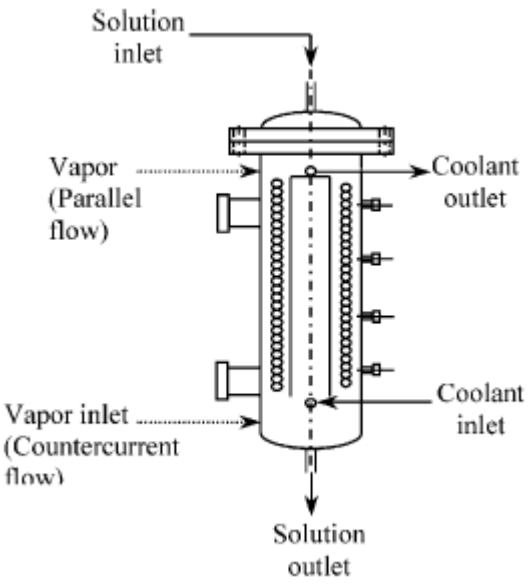

Figure 2.3: Helical coil thin film absorber [34]

Kwon and Jeong used a closed cycle for their investigations depicted in Figure 2.4. The supply tank is equipped with an electric heater to produce vapor at the desired conditions. The concentration of the vapor was calculated from the pressure and temperature condition in the supply tank. The concentration of vapor range 45% to 96% and the weak solution range 3% to 30%. The weak solution concentration was previously determined from temperature measurement and density with a pycnometer. The strong solution

concentration was calculated from mass and energy balances due to problems with the inline measurement. However the test rig consists of temperature sensors inside the test section to obtain temperatures of the thin film and calculate the exact heat transfer the heat transfer was calculated from inlet and outlet temperatures because it was not possible to measure.

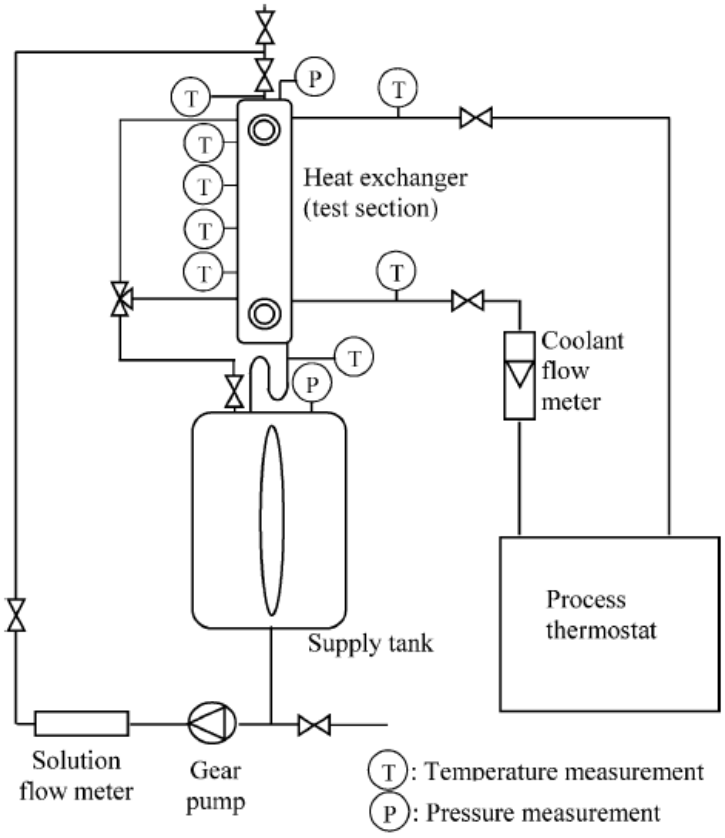

Figure 2.4: Schematic diagram of the experimental setup [34]

In all cases the heat transfer rate for parallel flow is greater than counter current flow. The difference increases with decreasing weak solution concentration due to the influence of vapor flow rate on counter current flow. The effect of vapor flow decreased with higher solution concentrations due to decreased specific volume of the vapor which results in decreased vapor velocity and interfacial shear stress. For counter current flow heat transfer deteriorates with increasing vapor flow. Therefore co current flow rate´s heat transfer is dependant from the solution and vapor flow rate. Heat transfer increases although it is laminar flow and the film thickness and therefore thermal resistance increases with solution flow rate due to better mixing and wetting. The effect of weak solution temperature is

negligible compared to other effects. Equally to the heat transfer the mass transfer rate for parallel flow is in any case better than counter current flow and also the difference becomes smaller with higher solution concentrations.

Equally to Kang 1999 the test facility produces low ammonia vapor concentrations. Confirming the calculated rich solution concentration with measuring is strongly recommended.

Garimella [10] designed a horizontal falling film absorber with microchannels depicted in Figure 2.5 and Figure 2.6. The coolant fluid flows upward counter current to the weak solution through microchannels. Due to the microchannel design heat transfer of the coolant is considerably increased. The solution enters the absorber from the top, distributed from a drip tray and flows through the latter of coolant microchannels. The ammonia vapor enters the absorber from the bottom counter current to the weak solution.

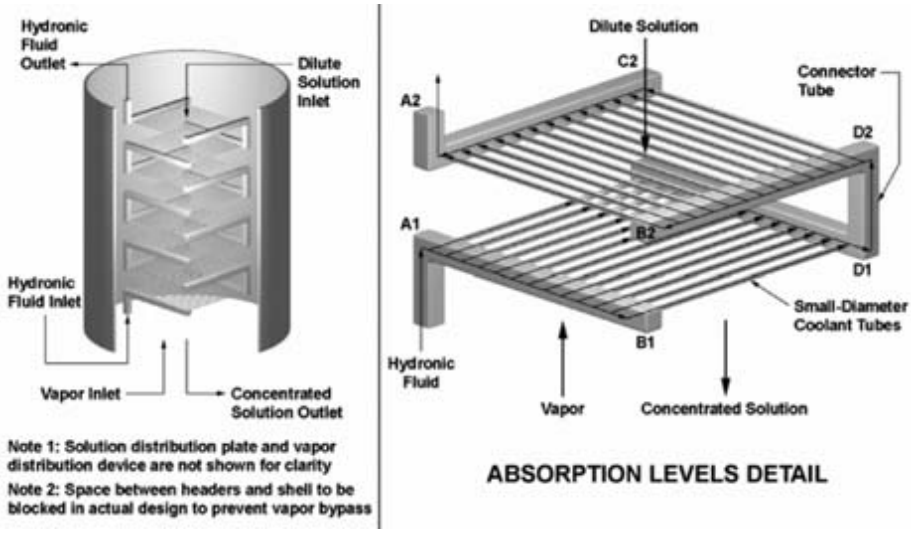

Figure 2.5: Microchannel heat and mass transfer concept Garimella [10]

Figure 2.6: Microchannel absorber views [10]

Garimella developed a numerical model to scale a hydronically cooled absorber. For the design conditions depicted in Table 2.1 the geometry design depicted in Table 2.2 were chosen.

	Inlet	Outlet
Pressure, bar	5.1	
Solution flow rate, kg/s	0.018	0.0284
Solution concentration	0.206	0.470
Solution temperature, °C	98.54	45.17
Vapor flow rate, kg/s	0.0095	0
Vapor concentration	0.995	
Vapor temperature, °C	38	
Coolant flow rate, kg/s	0.5	
Coolant composition	50% Ethylene glycol	
Coolant temperature, °C	42	52.79
Absorber heat duty, kW	19.28	

Table 2.1: Design conditions for miniaturized absorber

Tube outer diameter, mm	1.587

Tube inner diameter, mm	1.079
Tube wall material and conductivity	Carbon Steel, 60 W/m-K
Tube length, m	0.127
Number of tubes per row	40
Number of tube rows	75
Number of rows per pass	15
Tube transverse pitch, mm	3.175
Tube row with, m	0.12775
Row vertical pitch, mm	6.35015
Absorber height, m	0.476
Total surface area, m^2	1.9

Table 2.2: Absorber geometry of prototype

The results showed a high falling-film heat transfer coefficient (2790 W/m²K) similar to typical falling film absorber designs but even the coolant heat transfer coefficient (1604 W/m²K) was high due to the small pipes which is often the problem in traditional falling film absorbers.

According to the analytical investigations of Garimella [10] **Meacham and Garimella [37]** investigated the absorber design experimental. In addition to the original absorber design they provided a visual confirmation of the solution flow to find the optimum horizontal and vertical tube pitch which differed from the original design (4.76 mm vertical and horizontal tube pitch) to minimize bridge and column formation between adjacent tubes while having adequate flow area for the rising vapor. The geometry of the absorber prototype built is depicted in Table 2.3. Meacham and Garimella used a closed cycle to obtain the desired test conditions. The weak solution and vapor concentration were determined by pressure and temperature measurement in the desorber. No rectification was used to enrich ammonia vapor concentration. However ammonia vapor concentration was varied by desorber pressure and temperature. The rich solution concentration was obtained by a coriolis flow meter.

Tube outer diameter, mm	1.575
Tube inner diameter, mm	1.0679
Tube wall material and conductivity	T304 Stainless Steel, 15.4 W/m-K
Tube length, m	0.140
Number of tubes per row	27
Number of passes	5
Number of rows per pass	16
Tube transverse pitch, mm	4.76
Row vertical pitch, mm	4.76
Absorber height, m	0.508
Total surface area, m^2	1.5

Table 2.3: Absorber geometry of build prototype

Hence the coolant heat transfer coefficient was high and the absorber seemed solution heat transfer resistance controlled the results showed a linear increase in heat duty with increasing solution flow rate. The influence of vapor concentration and flow rate could not clearly be revealed due to the test apparatus design. The design goal could not be reached and Meacham and Garimella concluded the decreased surface area, low ammonia vapor concentration and flow distribution problems reasonable. Further investigations to visually observe the flow regime of the solution were addressed to clarify the disagreement of predicted performance and experimental results.

According to the experimental results for the prototype of Meacham and Garimella [37] the experimental results of heat and mass transfer were lower than expected from the numerical model. **Meacham and Garimella [38]** developed an analytical model to explain this deviation. They calculated the conditions within the absorber for every segment from the known coolant temperatures for every segment. Accordingly Meacham and Garimella added an effective area ratio to match the experimental results. An effective area ratio from 0.22 to 0.31 was calculated which means that only 22% to 31% of the total surface area was used for heat and mass transfer on the solution side and an improvement for the solution distribution has to be found.

Therefore **Meacham and Garimella [39]** extended the investigations with improved wet ability due to a drip tray depicted in Figure 2.7. The original drip tray was a perforated tray

with minor warping of the underside of the tray causing the solution to collect at desired locations before falling unevenly over the tube array. The new drip tray consisted of a stainless steel tray with perforations and small length tubing placed in each hole. These tubes ensure even solution distribution and prevent the solution from rivulet flows. The geometry of the absorber was slightly changed to include a big sight glass for flow distribution observation. Therefore the surface area was reduced to 30% of the prototype absorber.

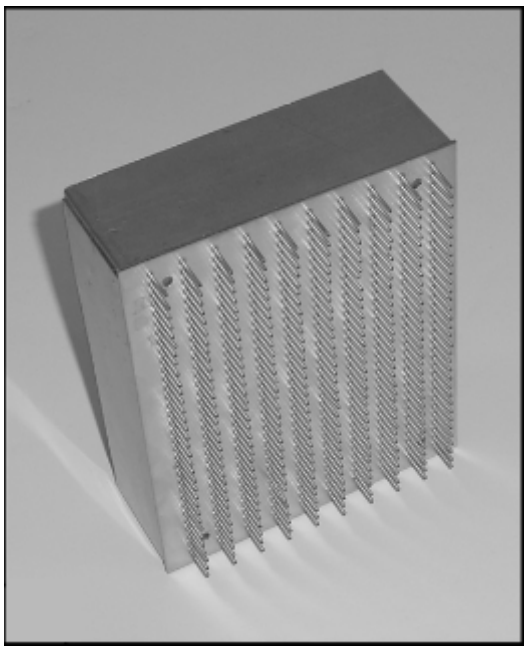

Figure 2.7: Improved drip tray [39]

The schematic of the test apparatus is depicted in Figure 2.8 and is identical to the apparatus from Meacham and Garimella [37]. The results showed that increasing solution, vapor and coolant flow rate increased the heat transfer coefficient and consequently heat transfer. In the original design the coolant flow rate had no influence on the heat transfer coefficient and Meacham and Garimella concluded that the decreased number of coolant pipes per row in the new absorber design led to turbulent flow and therefore increased heat transfer. The influence of coolant flow rate on the solution heat transfer coefficient could not be clearly depicted due to the overall determination and high error band for calculating solution heat transfer coefficient. Similar to further analytical investigations Meacham and Garimella [38] announced a segmental analysis like for the prototype absorber. However the results

showed that with only 30% of the original absorber design surface area the same heat duty could be transferred. They concluded that the enhanced solution distribution is the key parameter for the performance enhancement. This is proven through the increased solution side heat transfer in a range of 638 W/m²K to 1648 W/m²K in comparison to 145 W/m²K to 510 W/m²k for the prototype. The visual observation of the solution flow showed also a uniform distribution and supported the conclusions. The new absorber design was patented by Garimella in the United States [11].

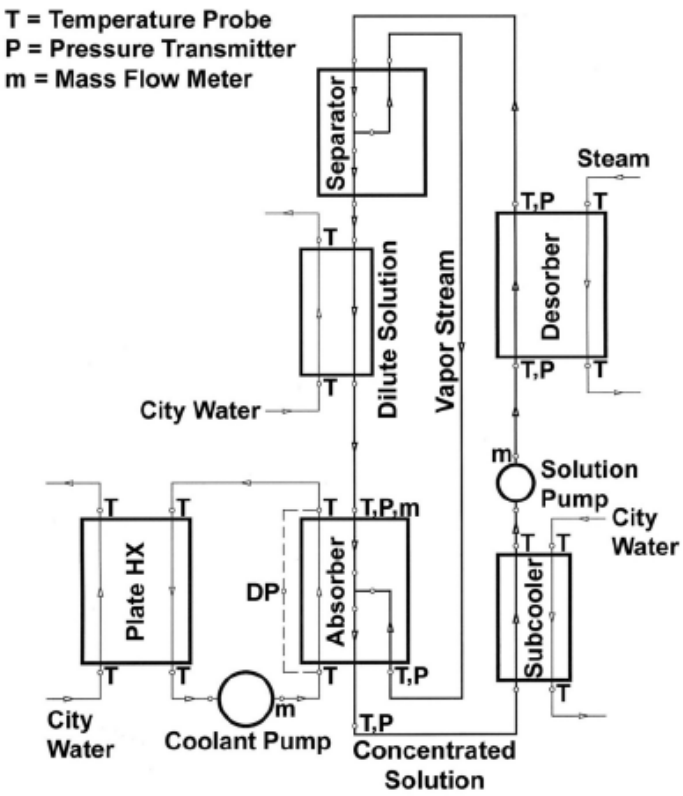

Figure 2.8: Closed cycle from Meacham and Garimella [39]

Goel and Goswami [12] proposed an improved horizontal tube absorber. They considered using the space between two horizontal tubes to enhance mass transfer area with a screen mesh/fabric and accordingly enhance the solution distribution over the coolant pipes. A liquid film is build between the horizontal pipes depicted in Figure 2.9. The screen can be made of aluminum, steel, stainless steel, glass, fiber and nylon but should be flexible to conform the shape of the coolant tubes. The material should have a good wetting characteristics and the size of the meshes should be considered to ensure a falling film over the mesh and prevent the formation of droplets.

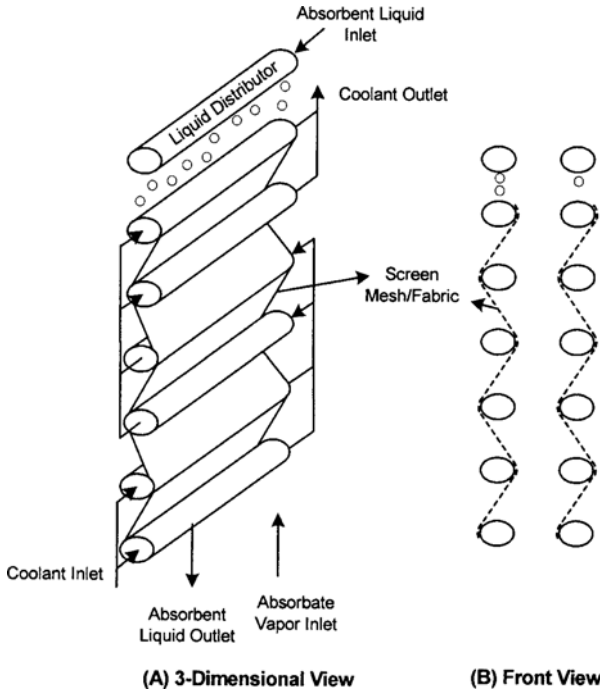

Figure 2.9: Schematic of screen/mesh fabric Error! Reference source not found.

The numerical model of the new design leads to an improvement of 20% less absorber size and has the advantage to be used in existing absorber designs.

Driven from the good performance of the numerical results of the improved falling film absorber **Goel and Goswami [13]** compared experimental the performance of a traditional absorber with the improved. The improved absorber is depicted in Figure 2.10 and a similar absorber was build without the screen mesh/fabric.

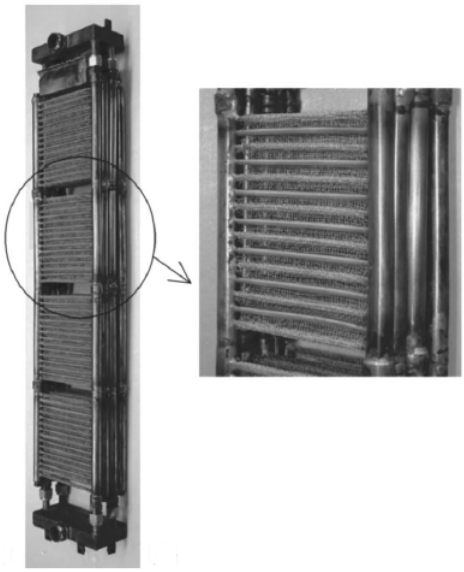

Figure 2.10: Improved absorber by Goel and Goswami [13]

First the absorber was tested without the enhancement and after that an aluminum screen mesh was fixed between the tube arrays. A closed cycle was used to compare the absorbers and obtain the desired conditions of coolant, ammonia vapor and solution depicted in Figure 2.11. Based on the test apparatus the ammonia vapor entering the absorber was around 96% and not as high as in typical absorber systems (99.5%). However they concluded from their numerical model that a slight decrease of ammonia vapor concentration has a negligible effect on the absorber performance.

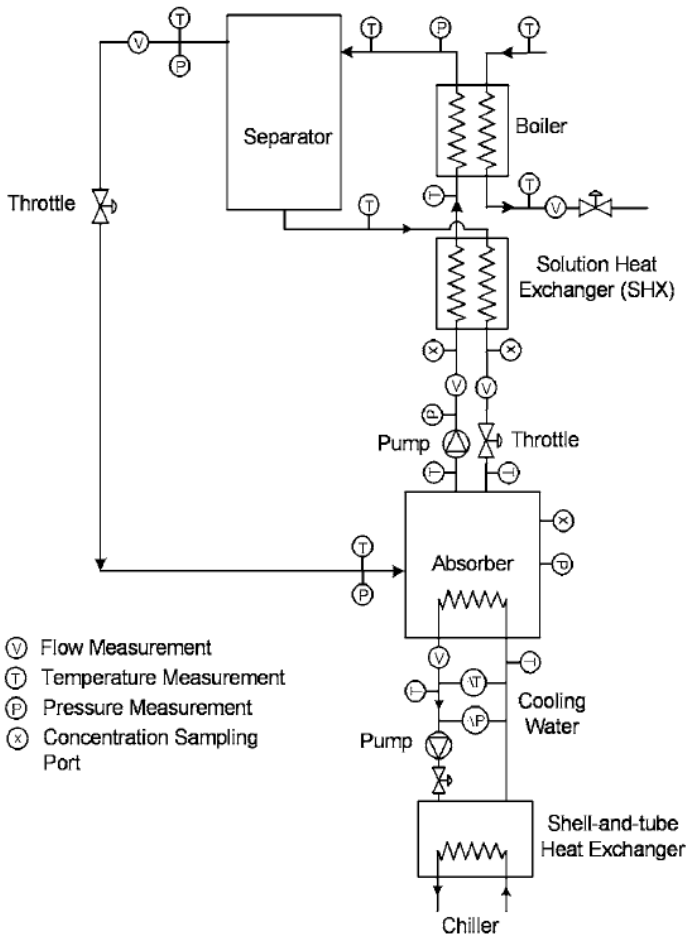

Figure 2.11: Schematic apparatus of Goel and Goswami [13]

The test conditions are depicted in Table 2.4 and solution flow rate and coolant temperature were varied to find their influence on absorption performance. Hence the wetted surface (A) could not be measured to determine the overall heat transfer coefficient (U) they only calculated the product (UA) to define the enhancement together with the heat duty transferred to the coolant.

Absorber pressure (bar)	2.81±0.02
Coolant medium	Water
	Absorber inlet conditions
Coolant mass flow rate (g/s)	88.7±1.7
Inlet coolant bulk temperature (K)	27.0±1.0
Weak solution mass flow rate (g/s)	14.46±0.424
Weak solution bulk temperature (°C)	43.0±1.0
Weak solution concentration (kg/kg)	0.30±0.015
Vapor bulk temperature (°C)	58.0±1.0
Vapor concentration (kg/kg)	0.956±0.004

Table 2.4: Baseline test conditions of Goel and Goswami [13]

The results showed an increase of heat duty of 20.5% with an error of 3.6%. They concluded the enhanced performance resulted from the aluminum screen mesh. However the residence time of vapor and solution was higher and the vapor flow rate was higher resulting in higher rich solution concentration. Another indication for increased performance was the product of mean overall heat transfer and surface area which increased 45% with an error of 16.8%. While increasing solution flow rate the heat duty for both absorbers increased due to increased surface wetting and mixing with ammonia vapor. The coolant flow was kept constant and Goel and Goswami concluded the heat transfer to be controlled by solution side heat transfer resistance agreeing their numerical model. The increase of heat duty could also be determined for the variation of solution flow rate in range 17% to 26%. The product of mean heat transfer coefficient and surface area kept constant for the variation of weak solution flow rate and was increased around 45% for the enhanced absorber. The influence of coolant temperature from 20°C to 30°C could also not be concluded for the product UA while the heat duty decreased with increasing coolant temperature due to the decreased absorption potential.

2.1.2 Relevant studies

Perez-Blanco [44] developed a model of an ammonia-water falling film absorber with horizontal tubes and confirmed it experimentally. He used overall mean heat and mass transfer coefficients and analyzed the influence of the different parameters. He concluded that the coolant heat transfer has no significant influence on the efficiency when it is over 2000 W/m^2K. The solution flow rate has no influence on the mass transfer because mass transfer is a surface phenomenon. A sensitivity analysis showed that only the mass transfer coefficient has a significant potential to increase the overall performance and therefore controls the efficiency of the absorber. Only in case of high solution temperature near the saturation the influence of the coolant heat coefficient becomes significant. Nevertheless the mass transfer coefficient is more significant.

A few more work exists in solving the coupled heat and mass transfer process within the ammonia-water absorption system. However the models describe only vertical falling film absorption neglecting wavy films and several parameters.

2.2 Bubble Absorption

Bubble type absorbers were strongly recommended for ammonia-water absorption systems instead of falling film mode because bubble-type provides high heat transfer coefficients and vapor distribution is easier than the liquid distribution needed in falling film absorbers [21].

Several attempts to model, numerically and analytically, the heat and mass transfer processes in bubble absorbers can be found in the literature.

2.2.1 Experimental work

Infante Ferreira [8] was one of the first investigating bubble absorption in a single vertical tube. He used a glass tube with an inner diameter of 10mm, 15.3mm, 20.3mm and the length was restricted to 1m to avoid high hydrostatic pressure losses. The tube was surrounded by a second glass tube to visually observe the absorption. Weak solution and ammonia vapor enter the test section from the bottom counter current to the coolant as depicted in Figure 2.12. To ensure similar heat transfer to the coolant as stainless steel pipes with water at a temperature of 25°C he used methanol as coolant with a temperature of -40°C. In order to avoid freezing at the outer tube and to measure the heat flux from the environment the methanol shell is surrounded by another tube with methanol at 25°C.

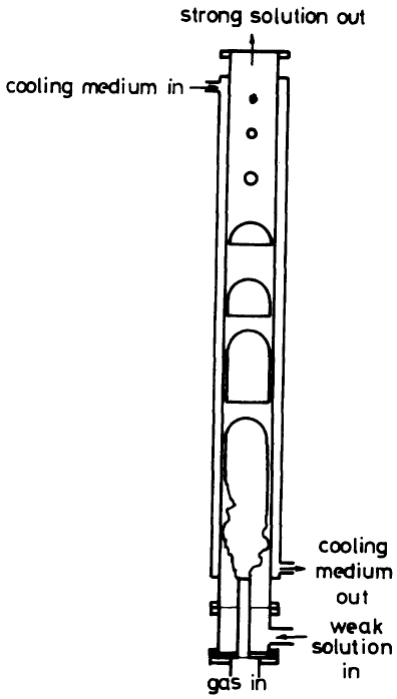

Figure 2.12: Test section [8]

Pure ammonia gas from a vessel is bubbled into the solution depicted in Figure 2.13 and even though the test rig offers the possibility to obtain co and counter current flow only co current upward flow was used due to unstable flow operations. The desired pressure in the system was obtained by heating the weak solution tank and therefore pressurizing. The solution cycle gives the possibility of subcooling the weak solution before entering the test section. While testing ammonia gas was purged from the vessel to obtain constant low solution concentration.

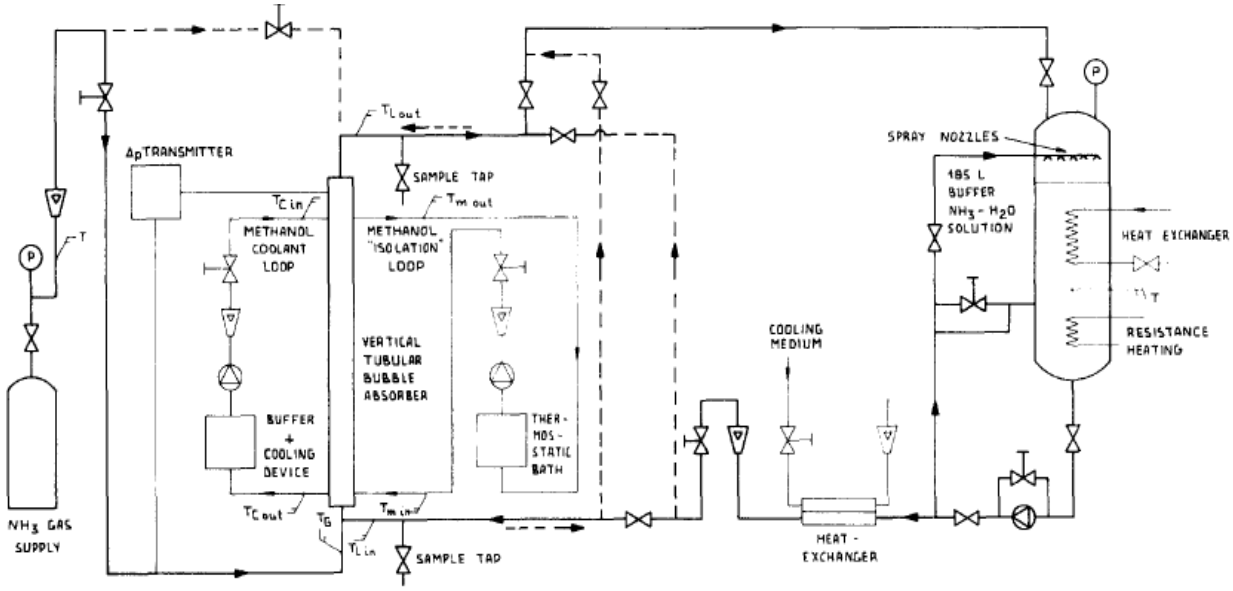

Figure 2.13: Schematic of the apparatus [8]

Several parameters were varied as summarized in Table 2.6. An annular type nozzle was used to insert the ammonia vapor from a 4mm inner diameter pipe in the center of the glass pipes. Infante-Ferreira concluded that the geometry of the nozzle has no significant effect on heat and mass transfer hence flow pattern changes rapidly after the entrance.

In order to calculate the predicted heat transfer coefficient α_i inside the tube Infante Ferreira divided the test section in two regions regarding to churn α_{Lf} and slug flow α_{Lp}. The fraction of each coefficient is determined by the void fraction ε

$$\alpha_i = \varepsilon \cdot \alpha_{Lf} + (1-\varepsilon)\alpha_{Lp}. \quad (2.1)$$

The heat transfer coefficient in churn flow at the entrance of the absorber is assumed to be equal to heat transfer coefficient in a cooled falling film proposed by Horn [15] and for the slug flow he assumed single phase flow in a tube.

The partial heat transfer coefficient in churn flow ranged 2810 W/m²K – 15630 W/m²K, the slug flow 310 W/m²K to 1120 W/m²K and the corresponding inner heat transfer coefficient 530 W/m²K to 12550 W/m²K. Infante-Ferreira concluded that the influence of the heat transfer coefficient at the solution side is significant when:

- The partial heat transfer coefficient α_c is high.
- The void fraction is relatively low therefore the heat transfer coefficient in the slug flow gains more influence.

The results were in good agreement to the measured values unfortunately these calculations require the estimation of the fraction of both flows and therefore visual confirmation of the whole test section is required.

Parameter	**Minimum**	**Maximum**
Diameter [mm]	10	20.3
$\dot{m}_v$ **[g/s]**	0.018	0.480
$\dot{m}_{ws}$ **[g/s]**	2.1	26.2
x_{ws}	0.341	0.451
x_{rs}	0.341	0.510
$\left(x_{rs} - x_{ws}\right)$	0.001	0.103
$\left(x_{ws,sat} - x_{ws}\right)$	0.005	0.170
T_v **[C]**	8.2	32
T_{ws} **[C]**	9.5	33.5
P [bar]	1.26	3.33

Table 2.6: Parameter variation [8]

In order to determine the mass transfer Infante-Ferreira used a common relation for mass transfer without simultaneous heat transfer which can be derived from dimensional analysis

$$Sh_{vL} = a\,\mathrm{Re}_L^{b}\,Sc_L^{c}\left(\frac{z}{D}\right)^{d}. \tag{2.2}$$

He gained the coefficients with a multiple linear regression and concluded that the gas phase velocity and the absorption height have a significant influence in mass transport while mass flow rate of the solution can be neglected. The influence of gas flow rate and therefore gas phase velocity correlates with the penetration theory proposed by Higbie [14]. If the gas flow rate increase, the liquid flow rate in the film increases, the mean and interfacial velocities in the film increase and the mass transfer coefficient also increases. Additionally Infante-Ferreira used a stepwise multiple linear regression method to obtain a function for calculating the absorber height z from the influencing parameters. For the range of tested parameters he concluded

$$z = 133.6\xi_L^{\,2.1}\cdot\dot{Q}^{0.6}T_L^{\,0.4}\dot{m}_G^{\,0.1}P^{-1}D^{-0.5}\dot{m}_L^{\,-0.04}. \tag{2.3}$$

Therefore regarding to equation 2.3 a higher pressure, larger inner diameter and increased solution flow rate lead to shorter absorbers. An Increase of liquid phase concentration, of liquid phase temperature, of the gas flow rate, and of the transferred heat leads to larger absorbers.

Merrill et al. [41] investigated the possibility of passive heat transfer enhancement techniques to compact bubble absorber designs. They concluded the coolant heat transfer, effective heat transfer and amount of refrigerant absorbed as the major influencing variables to enhance bubble absorber performance. Therefore Merrill et al. tested three different improved bubble absorber designs from their first design presented in Merrill et al. [40]. Frankly it was not possible to obtain this article. The original absorber had two enhancement techniques for heat transfer and one for mass transfer. The outside heat transfer coefficient was increased by manufacturing a wire spacer wrapped helical between the solution tube and cooling jacket thereby increasing coolant velocity and residence time. The solution side heat transfer coefficient was increased by repeated roughness of the inner

pipe to induce continual sublaminar boundary layer separation and reattachment [47]. Mixing tape inserts were attached into the inner pipe to break up bubbles into smaller sizes thereby increasing vapor-liquid interface. The original absorber design is depicted in Figure 2.15.

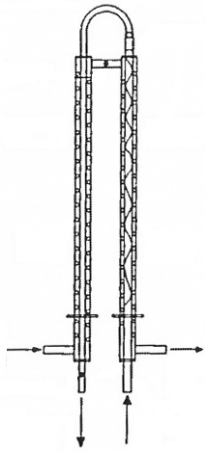

Figure 2.14: Original absorber design [41]

The absorber was tested for typical GAX load conditions depicted in Table 2.7.

Item	Specification
Approach delta T	8.9 C
Heat pump cooling capacity	3.52 kW
GAX absorber load	2.33 kW
System pressure	5.03 bar
Generator exit mass fraction	8%
Feed flow rate	4.92 g/s
Vapor mass fraction	99%
Vapor flow rate	0.91 g/s
Coolant flow rate	12.55 g/s

Table 2.7: Absorber specification [41]

The results showed that the heat transfer was controlled by the coolant heat transfer coefficient which was 2 times smaller (1863 W/m^2K to 4050 W/m^2K) than solution heat transfer coefficient.

To enhance heat transfer coefficient for the coolant flow the separation between consecutive spacers was reduced from 19.1 mm to 6.9 mm thereby increasing coolant velocity and coolant Reynolds number conclusively. To decrease the height of the absorber the original absorber with a height of 0.51 m was replaced by a series of five identical absorbers with a height of 0.254 m. To prevent flooding of ammonia vapor, which occurred with the original arrangement, the ammonia vapor was distributed with injectors in each absorber. To obtain the desired temperature difference the heat exchange area from 0.029 m2 in the original design to 0.087 for absorber 1. The absorber configuration is depicted in Figure 2.15. Overall the purpose of absorber 1 was to decrease the heat transfer resistance on the coolant side, increase heat transfer area and increase vapor flow rate.

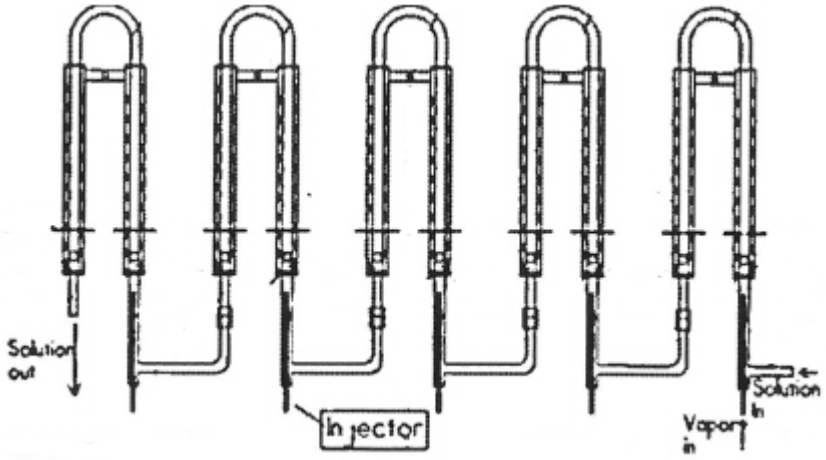

Figure 2.15: Schematic of absorber 1 [41]

The results showed that absorber 1 could not answer the expectations. The vapor flow could be increased by 34% but was still under the goal design. Furthermore the vapor flow rate with injectors was difficult to control. The absorber design has to be further improved to approach the desired temperature difference and GAX load as well.

The design of absorber 2 focused on increased vapor bubble residence time, simplification of the injection and increased heat transfer area. The internal and external improvements were the same as absorber 1. Only the ascending length of the absorber and the corresponding number of absorbers and injectors differed. By increasing the ascending length to 0.762 m and reducing the number of absorbers to two the heat transfer area increased to 1.05 m, a 20% increase over absorber 1. The reduction of injectors on the other hand simplified the vapor distribution. Equal to absorber 1 the goal could not be reached with absorber 2.

However the heat transfer coefficient increased and vapor distribution was simplified with increasing ascending length. The advantage could not be utilized to improve the performance due to poor vapor distribution.

Absorber 3 was a new design to neglect the pitfalls of absorber 1, the increased solution heat transfer resistance and the decreased bubble residence time. The ascending leg contained a fluted tube to increase the turbulence and therefore increase bubble residence time which results in increased heat and mass transfer. The descending leg was designed without a cooling jacket hence the GAX load in the original absorber was only one fifth of the ascending leg. Merrill et al. concluded the absence of bubbles in the descending leg due to buoyancy force which prevent bubbles from being dragged downwards as an explanation. The length of this single absorber was further increased to 1.27 m to increase heat transfer area. The absorber could also not fulfill the goal of GAX load like the other designs. Two different injectors were tested and the difference was significant concluding that the vapor distribution plays an important role hence it was also a problem in absorber 1 and 2.

Absorber 1 showed the best increase in GAX load, vapor flow rate and decrease in desired temperature difference hence vapor injection was crucial for this design. Simply adding two absorbers in a row like absorber 2 was no improvement. The new design of absorber 3 with the fluted tube had higher heat transfer coefficients on the solution side but the influence in the non cooled descending leg seemed to have a bad influence. Accordingly the difficulty in measuring heat transfer coefficients for the solution hindered the conclusions. Merrill et al. concluded to increase the inner diameter, create new injector designs and new static mixers to increase vapor flow rate to increase the performance of the bubble absorber.

Kang et al. [20] investigated visually the bubble behavior for different numbers and sizes of orifices, weak solution concentrations and vapor flow rates. Pure ammonia vapor bubbled from a pressurized vessel into the test section with weak solution at 0%, 10% and 20% ammonia concentration at a temperature of 22.5°C as depicted in Figure 2.16. The bubble diameter was visually measured with a high speed camera and recorded just after starting the test procedure ensuring that the measurement predicts the bubble diameter of the desired weak solution concentration.

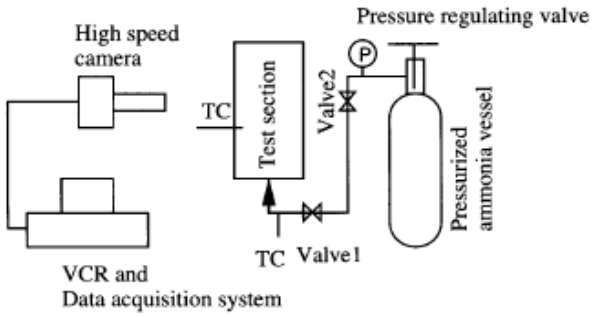

Figure 2.16: Schematic diagram of system apparatus [20]

The bubble diameter increased with increasing the orifice diameter increasing vapor flow rate and increasing weak solution concentration. Increasing weak solution results in decreasing absorption driving potential and therefore increasing bubble diameter hence increasing weak solution concentration decreases surface tension which usually results in decreasing bubble diameter for non condensable gases. Therefore Kang concluded that the absorption driving potential is more significant. The increasing bubble diameter as a function of vapor Reynolds number can be separated in two regions separated by the transition Reynolds number where the increase of the bubble diameter becomes smaller. In the first region the internal absorption potential denoted by the concentration difference is higher than the external absorption potential denoted by the vapor flow rate. Due to the larger bubble diameter at higher concentrations and therefore lower bubble velocity the transition Reynolds number increases with increasing weak solution concentration. The influence of number of orifices is insignificant only slight variations due to the vapor distribution occurred. The residence time increased with increasing weak solution concentration due to the decreased absorption driving potential. Kang used a statistic program to determine the coefficients for a non-dimensional correlation of the initial bubble diameter to orifice diameter

$$\frac{d_{ib}}{d_0} = 12.0\,\mathrm{Re}_v^{0.29}\,We_v^{-2.53}\left(Bu_v \times 10^6\right)^{2.58} x_{vl}^{-0.2} \tag{2.4}$$

where

$$x_{v1} = x_v - x_1\,. \tag{2.5}$$

The correlation estimates the initial bubble diameter with 20% error band.

In an additional work **Kang et al. [24]** investigated the correlation between bubble absorption and mass transfer. A similar test rig was used for investigation hence only one nozzle. The weak concentrations, pressure and orifice diameters were also adopted. Kang et al. divided the bubble absorption process in two parts the bubble growth before the detachment from the orifice and the bubble disappearance. He concluded a new correlation for the bubble diameter with a 15% error band including the Froude number and enabling to evaluate the mass transfer coefficient

$$\frac{d_v}{d_0} = 0.9 Fr^{\frac{1}{3}} x_{vl}^{-2} \tag{2.6}$$

Therefore the bubble diameter is calculated from the orifice diameter and thermal conditions. The mass transfer coefficient as a function of vapor Reynolds number is depicted in Figure 2.17 for bubble growth and in Figure 2.18 and as a function of Galileo number for bubble disappearance.

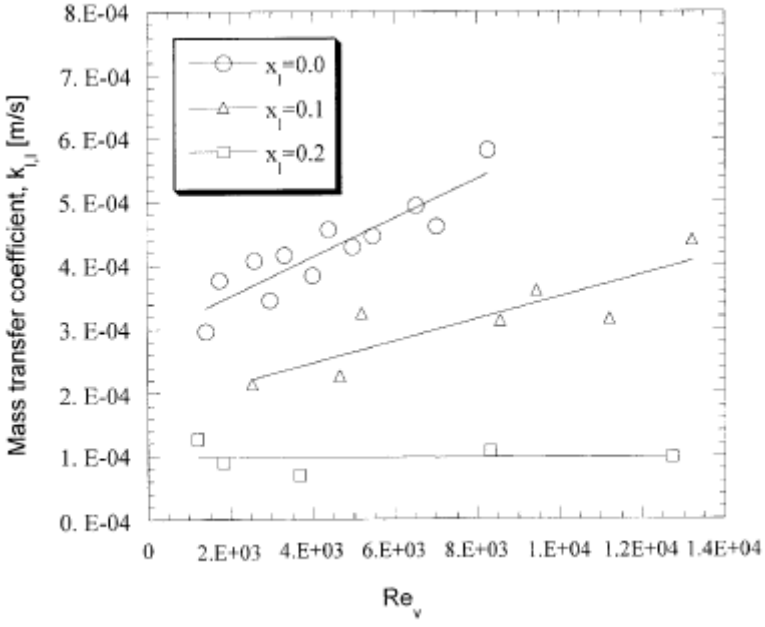

Figure 2.17: Mass transfer over vapor Reynolds number for bubble growth [24]

The vapor Reynolds number was replaced by the Galileo number in process II due to the different dominating forces. In process I the inertial force is dominant while the bubble is still growing and vapor flow rate´s influence is stronger than gravity force. During process II the buoyancy force is dominant and exceeds the influence of the inertial force.

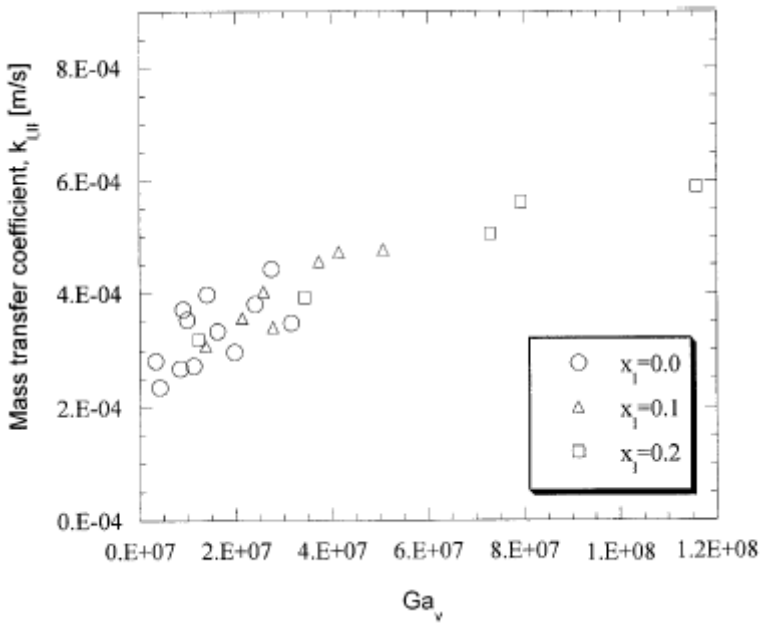

Figure 2.18: Mass transfer over of vapor Galileo number for bubble disappearance [24]

The bubble diameter and mass transfer coefficient increased linear for weak concentrations of 0% and 10% and was constant for 20% because of the decreasing influence of inertial forces due to decreasing absorption potential. The mass transfer increased with increasing Galileo number and is regardless of weak concentration.

Based on the experimental results Kang calculated the coefficients to express

$$Sh_{lI} = f\left(Sc_1, \mathrm{Re}_v, x_{vl}\right) \tag{2.7}$$

for process I and

$$Sh_{lII} = f\left(Sc_l, Ga_v, x_{vl}\right) \tag{2.8}$$

for process II. The results with an 18% error band were

$$Sh_{lI} = 0.131 \cdot Sc_1^{0.775} \cdot \mathrm{Re}_v^{0.597} \cdot x_{vl}^{6} \tag{2.9}$$

and

$$Sh_{lII} = 0.0155 \cdot Sc_l^{0.49} \cdot Ga_v^{0.52} \cdot x_{vl}^{4} \tag{2.10}$$

noting that this correlations only apply for the desired conditions.

Lee et al. [35] investigated the influence of flow rates on the absorption performance. He varied the solution flow rate, vapor flow rate and the concentration of the weak solution. The test facility is depicted in Figure 2.19. The vapor is in counter current flow to the weak solution and enters the test rig at the bottom from a pure ammonia vessel. The weak ammonia solution was obtained by mixing distilled water and ammonia gas. The concentration was calculated from conductivity measurements hence conductivity is a function of ammonia concentration.

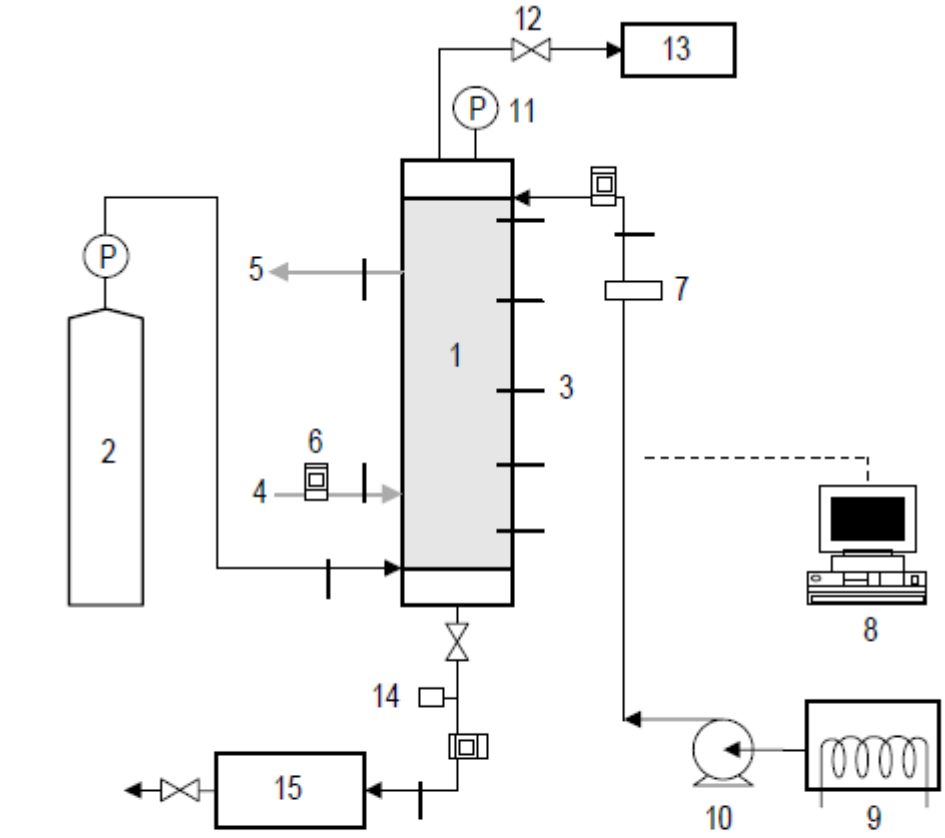

Figure 2.19: Test facility [35]

The test section consists of a plate heat exchanger treated with sandpaper depicted in Figure 2.20.

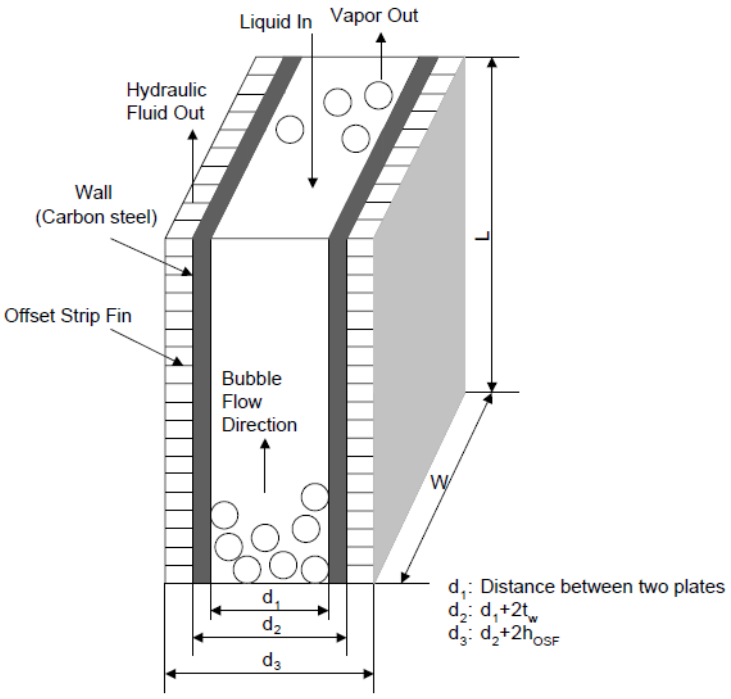

Figure 2.20: Test section Lee [35]

Lee figured out that increasing the solution flow rate results in a small increase of the mass transfer but heat transfer increases fairly. Increasing the vapor flow rate leads to increased heat and mass transfer performance. However ammonia gas was absorbed well the heat transfer performance was lower than heat generation performance.

Kim [30] carried out an experimental study to test a bubble absorber with low solution flow rates as needed in GAX cycles. As depicted in Figure 2.21 the test apparatus consists of a vapor supply line from a pure ammonia vessel, a weak solution line to distribute the solution from the top, a coolant line and a rich solution receiving line for neutralization. The system is pressurized by heating the weak solution and therefore no pump is needed to distribute the solution. The ammonia vapor is also distributed by heating. The weak solution concentration is obtained by titration method and the rich solution concentration by an ultra sonic measuring device. Thermocouples were included in every cooling jacket to measure local heat transfer and therefore read into local mass transfer. To gain lower deviation for the coolant mass flow Kim installed two mass flow meters in a row for low and high flow rates.

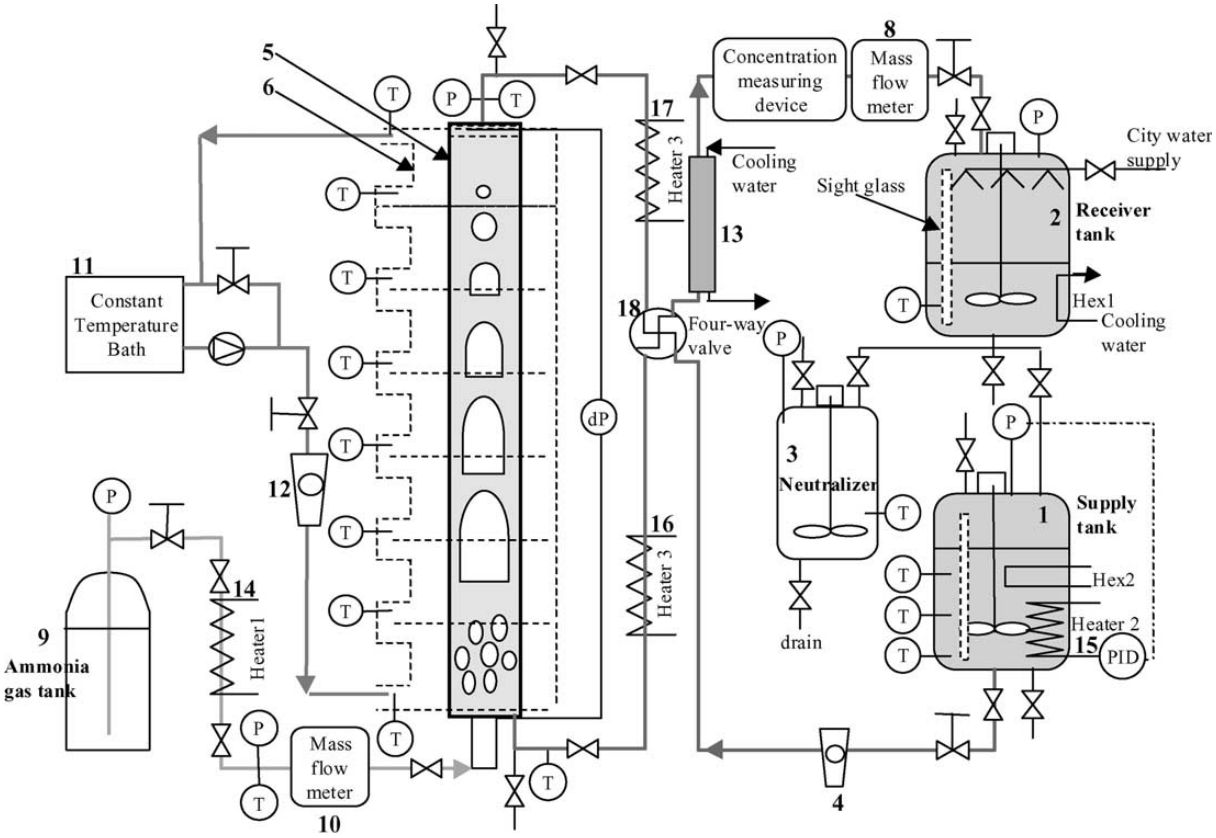

Figure 2.21: Schematic diagram of the test apparatus [Kim 1-2003]

He used a Pyrex glass with an inner diameter of 10 mm and 1500 mm length. The test section is surrounded by seven cooling jackets filled with cooling water made of poly-carbonate resin so that the whole test section is transparent and bubble absorption can be observed depicted in Figure 2.22.

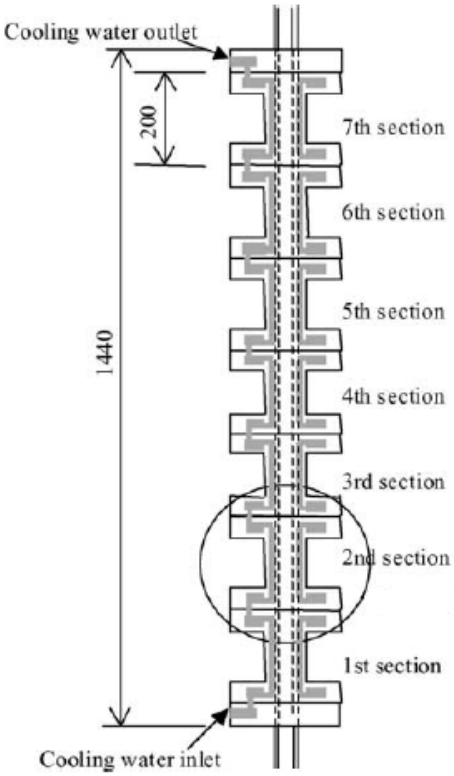

Figure 2.22: Test section Kim [1-2003]

Several parameters were varied to observe mass and heat transfer:

- Coolant temperature 20°C, 30°C and 40°C
- Coolant flow rate from 0.08 to 0.4 L/min
- Weak solution flow rate from 1.0 to 3.5 kg/h
- Ammonia gas flow rate 0.6, 0.9 and 1.2 kg/h
- Weak solution concentration 2.5, 10.3 and 21.6 NH_3 wt.%

Kim observed only two of the further mentioned flow patterns, at first the churn flow, followed by the major part of slug flow with well shaped Taylor bubbles. The task to work with low solution flow rates was complied well without any wetability problems. The absorption length decreases with increasing the weak solution flow rate and with decreasing the gas flow rate. Increasing coolant flow rate also decreased absorption length but is less sensitive. Hence Kim investigated the absorber performance for usage in a GAX cycle the influence of weak solution concentration and therefore decreasing absorption potential is minor to other parameters for 2.5 and 10.3 NH_3 wt.%.

Jenks [17] focused on investigating small scale bubble absorber for residential or mobile use. In order to achieve compact and light absorbers claimed for this area he built a microchannel absorber depicted in Figure 2.23. The ammonia vapor is distributed through a sintered porous plate or PEEK plates with different patterns of holes drilled to gain improved mixing of weak solution and ammonia vapor. On the other side he used a microchannel with 150µm, 400µm and 1500µm depth for the weak solution. The intention to use microchannels with a depth around thin film thickness was to benefit from the high heat transfer coefficient in falling film absorption. The surface of the microchannel was either smooth, cross ribbed, angle cross ribbed or streamwise finned.

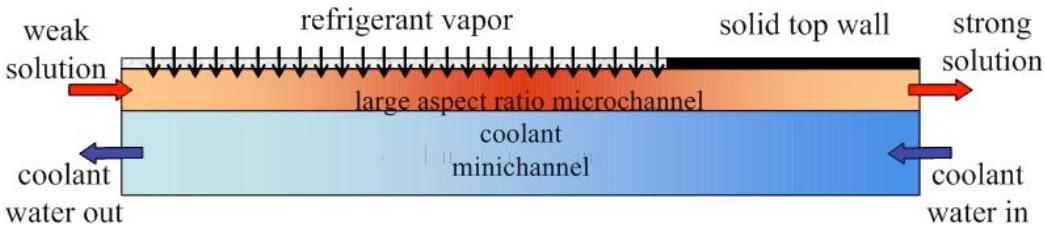

Figure 2.23: Schematic of a microscale bubble absorber [17]

The test facility depicted in Figure 2.24 consists of a solution, coolant and vapor distribution line. Pure ammonia vapor from a vessel is distributed into the test section and pressurized weak solution by an air pump circulates through the test section. No heater is included to obtain ammonia vapor or controlling weak solution pressurization. Temperature, pressure and flow rates for every line were measured together with a coriolis flow meter to calculate weak and rich solution concentration.

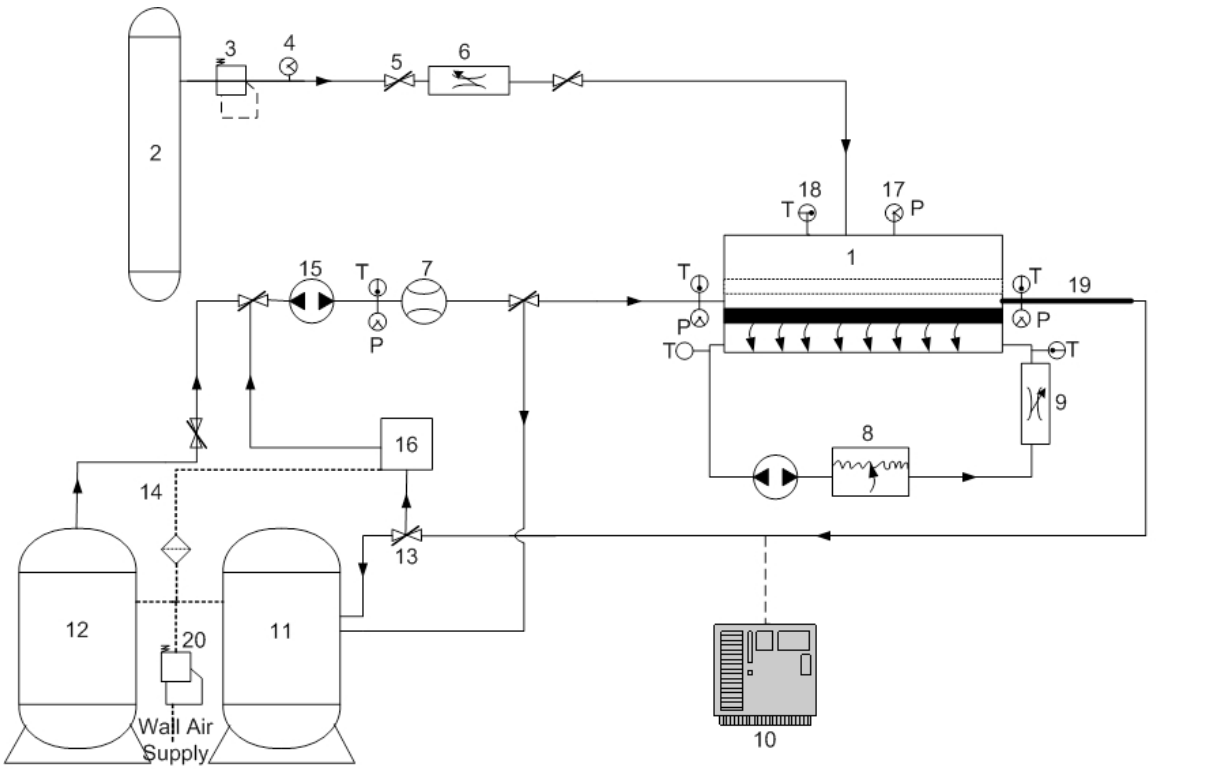

1. Absorber	6. Gas Flow Controller	11. Discharge Reservoir	16. Sample Reservoir
2. NH_3 Tank	7. Corriolis Flow Meter	12. Weak Solution Reservoir	17. Pressure Transducer
3. Pressure Regulator	8. H_2O Chiller/Recirculator	13. 3-way Solonoid Valve	18. Thermocouple
4. Pressure Guage	9. Rotameter	14. Filter	19. Visualization Section
5. Manual Valve	10. Data Acquisition	15. Gear Pump	20. Air Pressure Regulator

Figure 2.24: Schematic of the test facility [17]

Jenks varied weak solution and vapor flow rate, system pressure and weak solution concentration for the different vapor distributor and microchannel geometries. The distributors of PEEK plates with drilled holes tend to create big bubbles at the top of the microchannel and were ineffective in comparison with the sintered porous plate depicted in Figure 2.25 and Figure 2.26. Therefore further tests were made only with porous plate configuration.

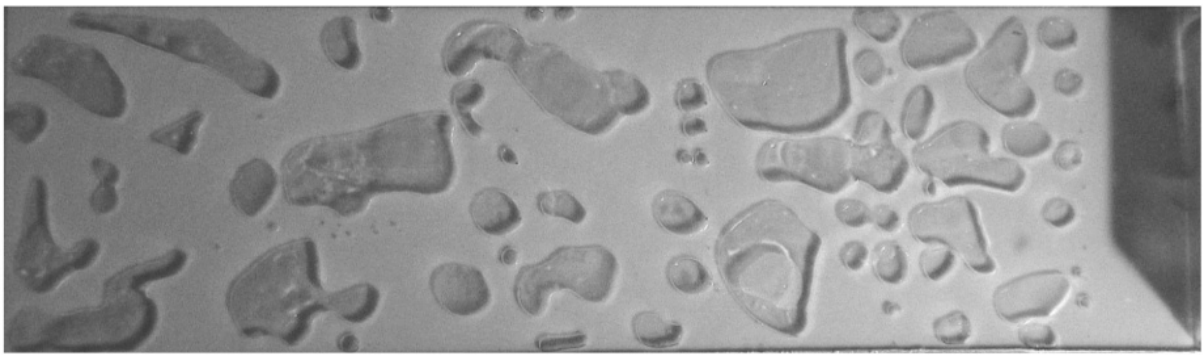

Figure 2.25: Bubble formation with PEEK plate and drilled holes [17]

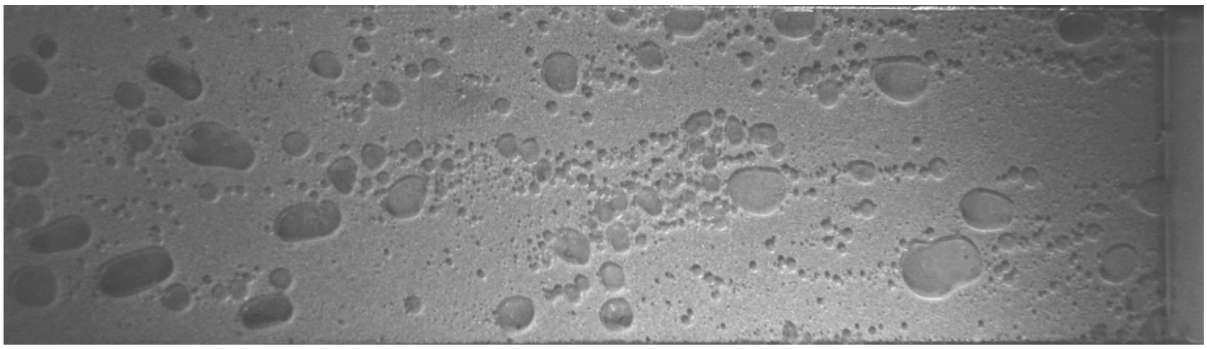

Figure 2.26: bubble formation with sintered porous plate [17]

The test results for the variation of the parameters showed no optimal channel depth for all desired conditions. Furthermore the different phenomena which influenced the mass and heat transfer varied in their dominance. For low solution and vapor flow rates and overall optimum conditions according to absorption potential by pressure and concentration difference an existing optimum was found between 400µm and 1500µm. The small amount of bulk solution at the bottom of the test section and therefore decreasing heat transfer to the coolant and mass transfer to the liquid film dominates the overall performance. Increasing vapor flow rate leads to bubbles touching the bottom of the test section and therefore decreasing heat and mass transfer area for 150µm and 400µm microchannels. Due to this disadvantage the 1500µm microchannel becomes better for high flow rates and the disadvantage of high bulk solution decreases. The surface enhancement of ribs and fins showed no overall performance increase. Therefore considering the optimal flow rates of 3g/min for ammonia vapor and 10g/min weak solution a microchannel depth of 400µm were concluded optimal. An infinite one dimensional model with assumption of instant absorption was designed to calculate the temperature and concentration profile along the absorber.

Cardenas [1] pursued the investigations of Jenks [17]. Based on the previous work he built a similar microscale absorber with a microchannel depth of 600µm smooth and with a stepped pattern. Hence no heater was included in Jenks´s test rig the desired temperatures for ammonia vapor, weak solution and coolant were limited. In order to extend the conditions to typical values and prove the performance of the microscale he built a more complex test facility depicted in Figure 2.27. Therefore it was possible to preheat the ammonia vapor and weak solution through the hot oil bath and afterwards control the exact temperature with the electric heater. Additionally a nitrogen vessel was used to purge the test facility after testing.

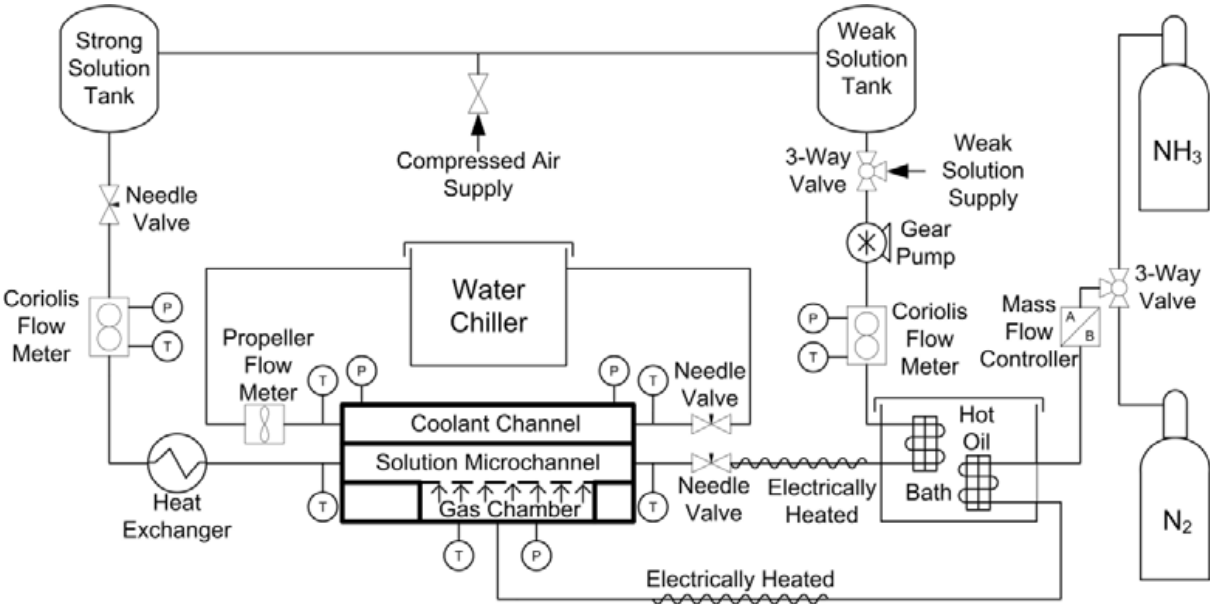

Figure 2.27: Schematic of the test system [1]

Coolant temperature, and flow rates of coolant, weak solution and vapor were varied. The experimental results were confirmed with a numerical model and further parameter studies were made. Additionally the pressure drop through the porous plate were measured and concluded to be significant and result in a pressure increase in the evaporator and therefore increasing evaporator temperature. Different from Jenks [17] Cardenas concluded that the best mass transfer performance could be obtained with a depth of the microchannel of 1.1 to 1.2 mm without losing heat transfer performance, taking into account the desired conditions. However Cardenas concluded that the predictions of his simplified one

dimensional program cannot fully describe the processes within the absorber and a more complex model would disprove this conclusion.

Cerezo [3] investigated the absorber performance of a plate heat exchanger und typical chiller conditions. The test facility depicted in Figure 2.28 consists of a coolant, solution and heating cycle. The pure ammonia was distributed from a vessel flowing co current to the weak solution which was previously heated before entering the test section. The strong solution and not absorbed ammonia vapor left the test section at the top, were separated and afterwards stored in the vessel (TA). Ammonia vapor was ventilated to the ambient. The absorber pressure was controlled by the amount of injected ammonia vapor and was kept constant at 1.6 bar.

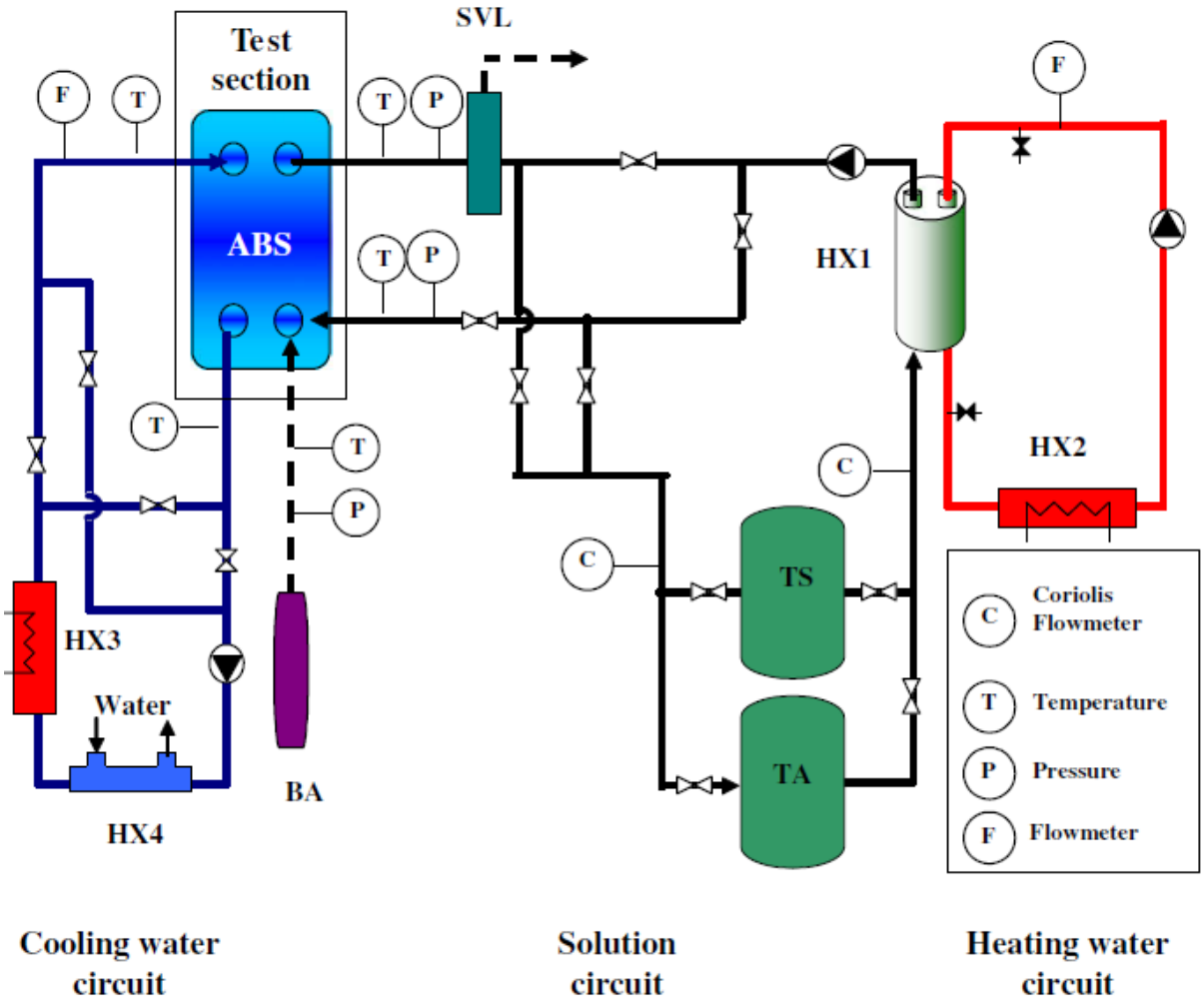

Figure 2.28: Schematic diagram of the test facility [3]

The concentration of weak and strong solution was calculated via density measurements by coriolis flow meters. Accordingly temperature, pressure and flow rates were measured.

The experimental results showed an increase in heat transfer when increasing weak solution flow rate hence better mixing of vapor and solution. The heat transfer was always greater for lower weak solution concentration due to the increased concentration difference and therefore absorption potential. The mass transfer coefficient kept constant with increasing solution flow rate and increased slightly for lower weak concentration. Equal to the heat transfer Cerezos results showed a higher mass transfer for lower weak solution. Decreasing cooling water led to increased mass and heat transfer due to the increased absorption potential. An increase of absorber pressure from 1.6 bar to 2 bar showed significant higher heat and mass transfer and Cerezo constituted this with the increased pressure gradient. However the saturation of ammonia solution depends on pressure and temperature and the absorption potential increases with increasing the pressure he did not mention its influence. The effect of weak solution temperature was negligible but could be explained with the low variation of 38°C to 42°C. An increase of coolant flow rate led to linear increasing of mass flux but had no influence on heat transfer.

2.2.2 Relevant studies

Infante-Ferreira [8] developed a model for vertical tubular absorbers using experimental mean overall heat and mass transfer coefficients to estimate the required absorber height for complete absorption. Kang et al. [18] proposed a design model for a bubble absorber with a plate heat exchanger to evaluate the mass and heat transfer resistance in both phases for the first time to find the optimum design conditions. Later Kang et al. [21] compared the thin film and bubble absorption finding that the heat and mass transfer is always better in bubble absorbers. Kim [29] developed a model to obtain local temperature, mass transfer and heat transfer values. His model agreed well with the experimental data found in Kim [28]. Heat and mass transfer was significant influenced by weak solution and vapor flow due to increased turbulence at the entrance. The mass and heat transfer was considerably greater at the entrance with frost flow compared to slug flow.

2.3 Surfactants and nano particles

The aforementioned disadvantage of wetability for thin film absorption could be decreased with the addition of surfactants. The solution flowing through horizontal tubes, along a vertical tube or in plate heat exchangers tends to rivulet flow. Accordingly the capillarity of the small channels in plate heat exchangers increases the wetability problem. The interfacial tension between solid and liquid and the surface tension of the liquid are the major influencing parameters. Both can be decreased by adding surfactants. Furthermore provide some surfactants the possibility of surface tension gradients and therefore increasing heat and mass transfer which is described as the Marangoni effect.

Möller and Knoche [41] investigated the influence of surfactants on the ammonia-water absorption system. They added two anionic tensides, two non-ionic tensides and the alcohol 1-octanol to enhance the absorption. Therefore in a test section with distilled water at a constant temperature of 20°C surfactants with a concentration lower than 1% were added. After distributing the ammonia to the test section absorption occurred until equilibrium is reached at the aforementioned temperature. With the ammonia pressure Möller and Knoche calculated the absorbed mass by the ideal gas law to 2.19g. The experiments showed no decrease in mass transfer with the anionic and non-ionic tensides concluding that the heat transfer due to lower surface tension and therefore better wetability could be increased. However no improvement in mass transfer was observed concluding that no tension gradients occurred. Adding 1-octanol alcohol led to higher mass transfer and Möller and Knoche concluded that an ammonia-sensitive solubility of the additive, resulting in a change of the surface tension, could explain the results. This is in contrast to previous investigations of other authors who related the Marangoni effect to islands of surfactants at the surface.

Kang et al. [22] investigated the influence of surfactants on ammonia absorption and provided an explanation for the Marangoni effect. They measured the surface and interfacial tension of ammonia solution with and without surfactants via the Wilhelmy plate method where a plate is dipped into the test section and the stress balance around the plate leads to the surface tension depicted in Figure 2.29. Accordingly he observed the Marangoni convection with a He-Ne laser.

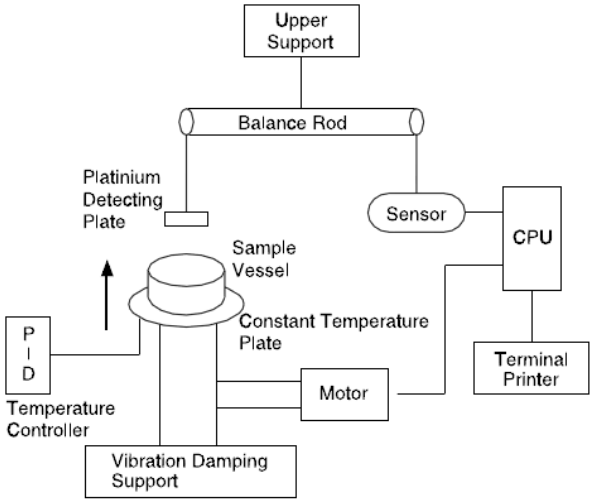

Figure 2.29: Schematic diagram of tension test facility [20]

The Marangoni effect described by Kashiwagi [26] is induced by surface tension gradients caused by islands of surfactants at the surface. Kang et al. disagreed finding that Marangoni convection occurred even without droplets of surfactants at the surface. They explained the Marangoni convection with the Radical-out model. Additives are added to the solution and some is adsorbed and some is dissolved. When ammonia vapor is injected the water molecules bind in NH_4^+ and OH^- ions hence the hydration force of ammonia is stronger than the adsorption force of the additive. As a consequence the alkyl radical of the additive is segregated from the bulk solution and moves to the surface leading to a significant reduction of the surface tension.

“When ammonia vapor starts to absorb into the solution, the surface movement is generated by the radical-out effect. In the surface wave, ammonia molecules gather on the crest region of the solution surface while water molecules at the trough region because ammonia has lower density than water. In the case without additives, there would be a surface flow from the crest region to the trough region by the characteristics of surface tension gradient of ammonia-water solution < 0. Therefore, the crest of the surface wave spreads out and the surface flow would be. In the case with additives, the surface flow is from the trough region to the crest region by the characteristics of surface tension gradient of the NH_3–H_2O solution > 0. Therefore, the surface flow becomes unstable and violent.”

Kang et al. named this effect “radical-out effect” hence the previous model of salting-out for $LiBr - H_2O$ proposed by Hozawa [16] is not an appropriate description for $NH_3 - H_2O$ systems.

The surface tension decreased significantly with increasing additive concentration until the solubility limit is reached in a range of 500 – 3000 ppm which depends on the additive used. Kang varied the NH_3 and LiBr concentration for fixed additive concentrations and concluded that the salting out effect is a trigger for Marangoni convection within the solubility of additives and surface and interfacial tension gradients are the trigger beyond solubility for LiBr. The variation of solution temperature showed no influence in surface tension and therefore no influence on Marangoni convection. However the interfacial tension varied with increasing ammonia concentration Kang et al. concluded no influence in Marangoni convection inducement from the visual experiments likewise the variation of solution temperature which kept almost constant. Marangoni convection was not observed for ammonia solution without additives but for some additives with a concentration of 500 ppm and nearly every additive with a concentration of 1500 ppm depicted in Table 2.8.

Additive	$\frac{\partial\sigma}{\partial x}$	Marangoni convection at $x_{add} = 500$ ppm	Marangoni convection at $x_{add} = 1500$ ppm
2E1H	>0	Yes	Yes
n-O	>0	Yes	Yes
2-O	>0	Yes	Yes
3-O	<0	No	Yes
4-O	<0	No	Yes
n-D	<0	No	No
2-D	$\geqslant 0$	Yes	Yes
3-D	$\geqslant 0$	Yes	Yes

Table 2.8: Concentration gradient of surface tension and Marangoni convection [20]

Excellent agreement was found between the positive concentration gradient of the surface tension and observation of Marangoni convection for 500 ppm concentration which is within the solubility limit. Therefore Kang concluded that this could be a criterion for the inducement of Marangoni convection within the solubility limit. Increasing the additive

concentration led to Marangoni convection even for additives where no convection was observed for 500 ppm concentration and Kang concluded that the higher concentration assists Marangoni convection but not induces it. Likewise Kashiwagi [26] Kang et al. summarized the magnitude of interfacial tension but found no influence in Marangoni convection and therefore concluded that the radical-out model proposed previously is the criterion for Marangoni convection inducement.

Later **Kang and Kashiwagi [23]** investigated the possibility of heat transfer enhancement by Marangoni convection by adding n-octanol. The purpose was to visually observe and confirm Marangoni convection and quantify the influence on heat transfer. A holographic interferometer was used to observe the Marangoni convection near the solution surface and to measure the time-dependant distributions of temperature and concentration in the solution. Pure ammonia vapor was injected from the top of the test section to absorb into a vessel with weak solution at a constant pressure of 2 bar and a temperature of 20°C. Five minutes after absorption started the coolant pump was turned on to reject the heat.

The solution concentration in the vessel increased due to ammonia absorption and therefore the influence of decreasing absorption potential on heat transfer increasing additives could be observed. From temperature profiles Kang and Kashiwagi observed that the diffusion boundary layer (DBL), the part of solution were absorption occurred, increased with additives and therefore heat transfer increased. He visually confirmed this by Marangoni convection starting just after injecting the vapor. The effect decreased with time due to the decreasing absorption potential. Likewise time dependant decrease of absorption potential the increase in heat transfer decreased with increasing weak solution concentration. Accordingly increasing additive concentration also increased heat transfer. The absorption heat transfer was enhanced 3.0 to 4.6 times with additives.

Kim et al. [30] continued the investigations of Kang et al. [23] and tested several additives for different ammonia concentrations. His purpose was to find the optimum additive, its concentration and ammonia concentration to enhance the absorption process. He used the same experimental apparatus as Kang [23] to investigate the absorption rate and surface tension for 2-ethyl-1hexanol, n-octanol and 2-octanol. The ammonia concentration tested was 0%, 8%, 14.3%, and 18.7%.

The experimental results showed for every additive an increase of absorption rate with increasing surfactant concentration. After reaching the maximum rate which concluded Kim et al. as the solubility limit the absorption rate decrease hence the barrier effect becomes dominant decreasing absorption rate. The absorption rate for each surfactant was the greatest for 8% ammonia concentration. However the absorption potential decreases from 0% to 8% ammonia concentration the effect of surfactants increases. From the visual results Kim et al. found that the bubble diameter increased with adding surfactants due to the decreased surface tension. Marangoni convection could not be observed like in the pool type investigations from Kang [23]. Kim et al. concluded that high vapor velocity and that the surface between vapor and solution only exists until bubbles disappear could explain the absent of Marangoni convection. The surface tension decreased significant with additive concentration until the solubility limit is reached and becomes constant afterwards. The solubility is the lowest for pure water and increases significant for 8% ammonia concentration. This could be the explanation why the absorption rate is greatest for 8% ammonia concentration. Kim et al. defined the absorption ratio as the mass of absorption with additive over the mass of absorption without additive. The maximum effective absorption ratio was 4.81 for700 ppm 2E1H and 18.7% ammonia concentration. Overall the absorption ratio increased with increasing ammonia concentration concluding that the enhancement through surfactants increases with decreasing absorption potential. A correlation for the surfactants was developed to predict the effective absorption ratio for the desired conditions with error band 15% for 2E1H and 10% for n-octanol and 2-octanol.

In addition to the investigations of Kim et al. [30] the possible enhancement of nano particles were investigated by **Kim et al. [31].** The same test rig and ammonia concentrations were used and the influence of copper, copper oxide and aluminum oxide with concentrations in the range 0.0 – 0.1 wt% on the mass transfer was determined. The average diameter of the nano particles were 50 nm, 47 nm and 33 nm.

The visual results showed that bubble diameter and the bubble rise decreased with nano particles. Also the shape of the bubbles changed from hemi-spherical to spherical with nano particles. The absorption rate increased quite linear with increasing nano particles concentration. The most effective absorption ratio of 3.21 was found for 18% ammonia and the maximum nano particle concentration of 0.1% of copper. Equal to surfactants the

influence of nano particles increase with decreasing absorption potential. A correlation for the influence of the nano particles was developed to predict the effective absorption ratio for the desired conditions with error band 10%.

In order to combine the findings of their previous works to enhance mass transfer with surfactants [30] and nano particles [31] **Kim et al. [32]** investigated the combination of both enhancements. Regarding to their previous works the same test facility was used to obtain absorption rates, surface tension and visually observe the bubble behavior. Equal surfactants and nano particles were added to equal ammonia concentrations. The results with surfactants and nano particles added to the solution showed similar results like adding only surfactants concluding that the influence of surfactants is more dominant than nano particles. The absorption rate was greatest for an ammonia solution concentration of 8%. Furthermore the absorption ratio of 5.32 was the greatest for the highest ammonia concentration of 18.7%, 0.1% CU and 700 ppm 2E1H. Kim et al. concluded similar to previous investigations that the enhancement of nano particles and surfactants is the greatest for high ammonia concentration resulting in low absorption potential.

Ma et al. [36] investigated the influence of nano particles called carbon nanotubes [CNTs] on heat and mass transfer in ammonia-water absorption. Inspired by Kim et al. investigations [31] and the great potential of heat and mass transfer enhancement Ma et al. continued this idea. However the chemical reaction of copper and aluminum with ammonia base was not considered. Therefore Mae et al. focused on nano particles which seem chemical resistant to ammonia base. The surface of the CNTs with a diameter of 20 nm and a length of 5 to 10 µm were modified by nitric acid and afterwards agitated by an ultrasonic applicator for 2 hours to distribute the CNTs evenly as depicted in Figure 2.30.

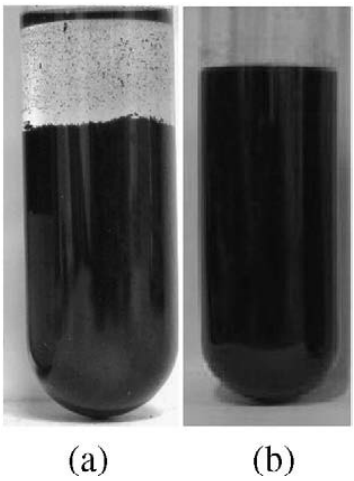

Figure 2.30: Pristine CNT (PCNT) and treated CNT (TCNT) [36]

Even after 3 days the TCNTs were well distributed while the PCNTs were mostly at the bottom and transparent solution at the top. The test facility consists only of an ammonia vapor distribution line as depicted in Figure 2.31. The weak solution is previously filled into the test section with a concentration of 0%, 7.36%, 14.08%, 20.23% and 24.08%.The test section with an inner diameter of 20 mm and a length of 200 mm is filled with weak solution and its weight is measured. The absorption rate is calculated from the time dependant weight gain while the vapor flow rate was kept constant.

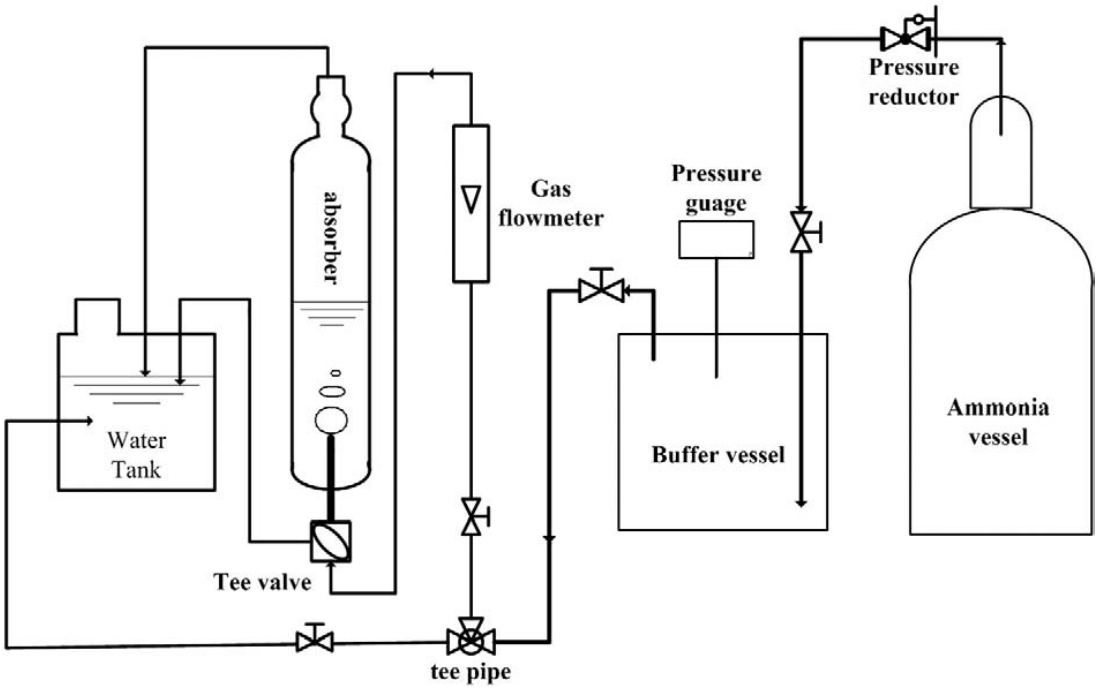

Figure 2.31: Schematic of the apparatus [36]

The absorption rate for each weak solution concentration increased at first with increasing CNT concentration and afterwards decreased. For the absorption ratio this trend is the same and significant for ammonia concentrations over 14.08%. This result is in contrast to Kim 2-2006 who concluded an increase of absorption rate with increasing nano particles concentration. However Kim only tested low concentrations of nano particles and never reached the maximum. Therefore Mae et al. concluded an optimum concentration of CNTs. The correlation between CNT concentration and absorption ratio can be explained with the four simultaneous appearing forces induced by the CNTs.

CNTs can cause the micro-convection in the ammonia solution because of the Brownian motion of nano particles. Regarding to Krishnamurthy et al. [33] the effect increases at first with increasing nano particle concentration and then decreases.

CNTs can cause the grazing effect described by Kars et al. [25]. The particles within a liquid adsorb the gas at the gas-liquid interface and deliver the gas into the bulk liquid. The grazing effect increases at first with increasing nano particle concentration and then keeps constant. This effect cannot totally be confirmed with experimental results.

Fan et al. [5] found that the gas hold up is increased due to the nano particles against pure water. Therefore increasing the gas-liquid interface and increasing absorption.

CNTs can improve the thermal conductivity of the liquid. Hence ammonia absorption is a correlated heat and mass transfer process and an increase in heat transfer leads to an increasing absorption potential therefore increasing absorption rate.

At last the vapor flow rate was varied and showed only little effect on absorption ratio. Mae et al. concluded that primarily the grazing effect is affected due the enhanced motion and exchange of CNTs at the liquid-gas phase.

2.4 Test rigs

The Arrangement of the test rigs can be separated in three different groups, the closed, the half closed and the open cycle. Dependent on the desired amount of weak solution, ammonia vapor and desired conditions each cycle has its advantages and disadvantages explained in this chapter.

2.4.1 Closed cycle

The closed cycle consists of every part of a complete absorption machine just without an evaporator and condenser depicted in Figure 2.8. Ammonia vapor is produced in a desorber, separated in the separator and flows together with the weak solution into the test section. Several heat exchangers can be assembled to ensure the desired temperatures of weak solution and vapor. The advantage of this cycle is the wide range of parameters which are able to be investigated. The amount of ammonia needed in a closed cycle is as well lower for high solution and vapor flow rates due its closed cycle. The disadvantages of this cycle are the costs, the complexity and the effort to produce pure ammonia vapor. Mostly the disadvantage of lower ammonia vapor concentration is accepted. The closed cycle is often used when a complete absorber is tested.

A modification of the closed cycle is a half closed cycle where the rich solution is neutralized and is not flowing back to the generator.

2.4.2 Open cycle

The open cycle consists of two separated distribution tanks as depicted in Figure 2.19. Pure ammonia gas is distributed by a vessel and the weak solution is mixed in a tank. The pressurizing is obtained by heating the weak solution and therefore evaporation. Jenks [17] and researchers after him used an air compressor to pressurize the weak solution and rich solution tank. The tests belonging to bubble absorption were mostly single pipe test rigs with small amount of solution and vapor and therefore an open cycle was used. The advantage is the simplified test rig and the simple possibility to obtain the desired conditions. For larger absorbers or longtime tests the disadvantage of using pure ammonia gas and mixed weak solution overweight the simplification.

3 Test Rig

The investigations of thin film absorbers in the last 10 years concentrated mostly on solving the wet ability problems occurring with the distribution of weak solution by drip trays [39] mesh fabrics [13] or surface treatments [41].

This investigation focuses on elemental understanding and analyzing the processes within the absorber. Therefore the decision was made to design a bubble absorber test rig referring to Kang [21] who concluded bubble absorption to be the best solution for the working pair of ammonia-water. Ferreira [9] concluded that there is an existing optimum inner diameter of the inner tube and later Fernández-Seara [6] concluded similar results with parameter analysis finding that there is an existing optimum inner diameter around 35 mm. Therefore a test rig is designed to test different diameters, co and counter current flow to observe absorption, bubble flow and measure the important parameters. Considerably lower inner diameter than 35 mm were used to show the expected heat and mass transfer in plate heat exchangers. The plate heat exchangers that will be investigated in further studies have a calculated inner diameter of 3.5 mm to 5 mm.

3.1 Layout of the test facility

Figure 3.1 depicts the schematic diagram of the test facility. As explained previously an open cycle is assembled for the investigations. The ammonia vapor is distributed from a vessel and therefore only 100% ammonia vapor can be tested. Usual ammonia-water absorption systems contain of a rectification to obtain 99% ammonia vapor and the deviation is neglected. According to the 4-way valve the weak solution can be distributed from the bottom or the top to test counter and co current flow against the vapor. The coolant is distributed from the top of the test section. After the test section the enriched solution is stored in a storage tank for further tests or neutralization in the following tank. The pressurizing is made by an air compressor according to Jenks [17] test rig. Further heat exchanger can be assembled to expand the variety of thermal conditions.

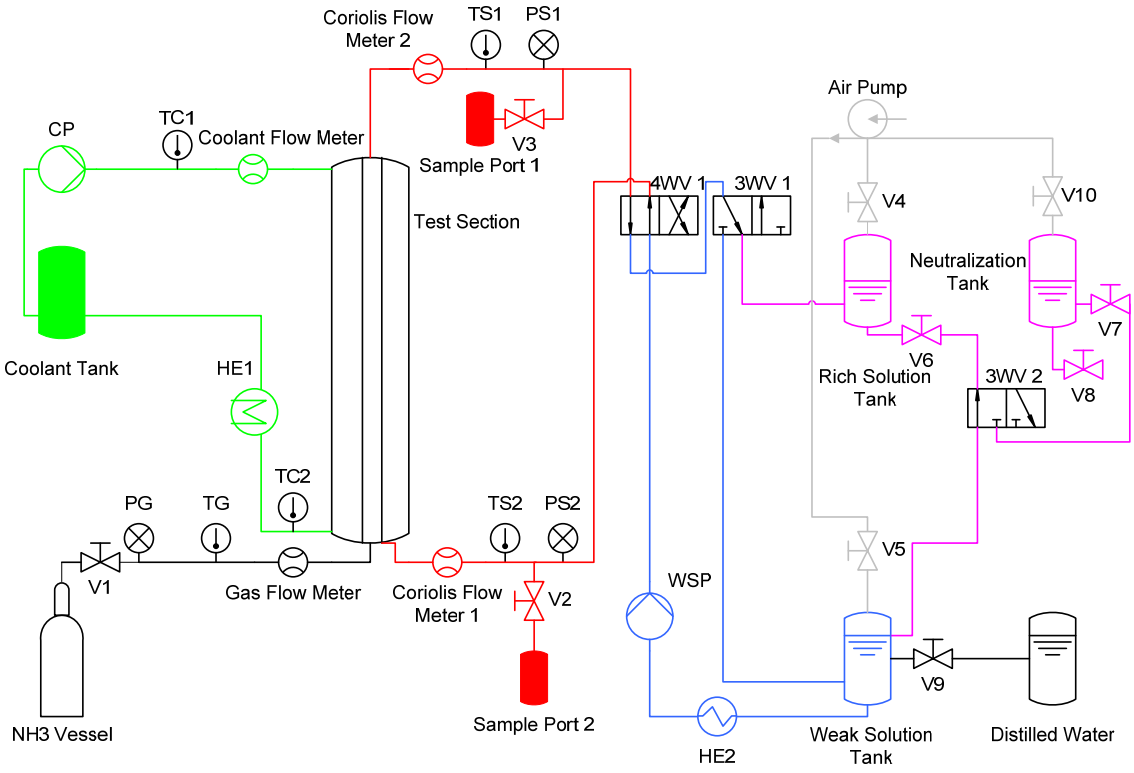

Figure 3.1: Schematic diagram of apparatus

3.2 Layout of the test section

The test section with a length of 1 meter to reduce hydrostatic pressure drop consists of a dual pipe depicted in Figure 3.2. The outer tube is filled with coolant water and in the inner pipe the weak solution and ammonia vapor flow co or counter current. For the inner tube a solution has to be found to obtain high heat transfer and a visualization of the bubble flow. Therefore the inner pipe consists of acryl glass at the bottom, middle and top and two stainless steel pipes as depicted in Figure 3.3 and Figure 3.4 for the size of ID14. The stainless steel pipes are stuck into the acryl pipes. The complete pipe is plugged into a reducer for the desired diameters depicted in Figure 3.5.

Figure 3.2: Dual pipe design of the test section

Figure 3.3: Inner pipe construction for ID14

Figure 3.4: Stainless steel and acryl glass pipe combination

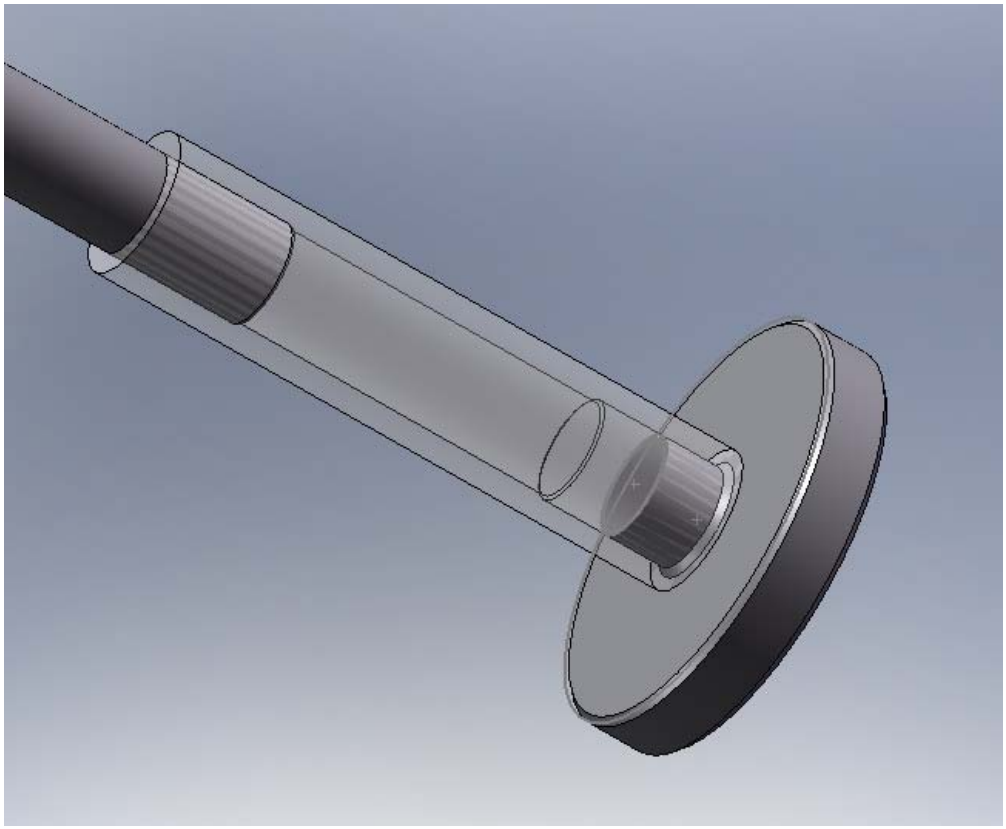

Figure 3.5: Acryl glass pipe and reducer

The assembling of acryl glass and stainless steel pipes can be varied. The decrease in heat transfer from the acryl pipes can be evaluated by testing a single stainless steel pipe for the same parameters. Accordingly a single acryl glass pipe can be used to evaluate the different bubble flow patterns. Especially the influence of different nozzles to the flow patterns could be observed and by means of heat and mass transfer evaluated with a single steel pipe. The addition of surfactants and nano particles is also possible hence only one solution pump is included in the solution cycle and no disturbances of vapor production is possible.

3.3 Test facility measurements

As depicted in Figure 3.1 several parameters are measured. The temperatures in the test facility are measured by t-type thermocouples. The coolant flow is obtained by a flow meter and regarding to the desired inner diameters and therefore coolant flows two flow meters for low and high flow rate should be considered. The pressure in the solution flow is measured and controlled by pressure transducers. The weak solution and rich solution flow rate and density are obtained by two coriolis flow meters to calculate the concentration of the solutions. A summary of possible common measuring devices is depicted in Table 3.1. Two sample ports can be used to verify the concentration by titration method.

Quantity	Device	Model	Range
Inlet coolant temperature T_{c1}	Thermocouple	T-Type	−200 to 350 °C
Outlet coolant temperature T_{c2}	Thermocouple	T-Type	−200 to 350 °C
Coolant mass flow $\dot{m}_c$	Flow meter	FCH-m-POM	0.015 – 1.0 l/min
Ammonia vapor temperature T_v	Thermocouple	T-Type	−200 to 350 °C
Ammonia vapor pressure p_v	Pressure transducer	PX482A-200GI	0-13.8 bar
Ammonia vapor mass flow $\dot{m}_v$	Flow meter	F-101D/F	2.1 l/min
Weak solution temperature T_{ws}	Thermocouple	T-Type	−200 to 350 °C
Weak solution density ρ_{ws}	Coriolis flow meter	ACM300	
Weak solution pressure p_{ws}	Pressure transducer	PX482A-200GI	0-13.8 bar
Weak solution mass flow $\dot{m}_{ws}$	Coriolis flow meter	ACM300	83-5000g/min
Rich solution temperature T_{rs}	Thermocouple	T-Type	−200 to 350 °C
Rich solution density ρ_{rs}	Coriolis flow meter	ACM300	
Rich solution pressure p_{rs}	Pressure transducer	PX482A-200GI	0-13.8 bar
Rich solution mass flow $\dot{m}_{rs}$	Coriolis flow meter	ACM300	83-5000g/min

Table 3.1: List of measuring devices

3.4 Materials

Acryl glass has a good resistance against basic chemicals such as ammonia solutions even at high concentration. The heat resistance is limited to 70°C for long-term usage and therefore a good heat transfer to the coolant has to be ensured. A long-term usage with water over 40° C can lead to water absorption and therefore discoloration of the acryl glass. The discoloration can be reversed by drying the pipe

The pressure stress durability of acryl glass is significantly lower than stainless steel and hence is only detailed calculated for acryl glass.

The acceptable pressure p_{acc} by Mohr is calculated with

$$p_{acc} = \frac{2s(d_o - s)}{d_o^2} \cdot \sigma_{acc}, \tag{3.1}$$

where s is the thickness, d_o is the outer diameter and σ_{acc} is the acceptable tension of the acryl glass pipe. Transforming the equation to s leads to

$$s = \frac{d_o}{2} - \sqrt{\frac{d_o^2}{4} - \frac{p_{acc} \cdot d_o^2}{2 \cdot \sigma_{acc}}}. \tag{3.2}$$

The acceptable tension for extruded acryl glass pipes, which is the common manufacturing process for small inner diameters, is according to a paper of Evonik Industries [4] 2.5MPa. With a maximum pressure of 0.6MPa in the inner pipe and outer diameters from 5 to 40mm the following minimum thickness is calculated as depicted in Table 3.2.

outer diameter [mm]	pressure [Mpa]	acceptable tension [Mpa]	minimum thickness [mm]	performed thickness [mm]	inner diameter [mm]
5	0.6	2.5	0.7	1	3.0
7	0.6	2.5	1.0	1	5.0
15	0.6	2.5	2.1	3	9.0
20	0.6	2.5	2.8	3	14.0
25	0.6	2.5	3.5	4	17.0
30	0.6	2.5	4.2	5	20.0
35	0.6	2.5	4.9	5	25.0
40	0.6	2.5	5.6	6	28.0

Table 3.2: Thickness of acryl glass pipes

According to the acceptable tension for steel the thickness could be around 0.1mm but due to manufacturing a thickness of 0.5mm is used when it is ensured that high precision pipes are obtained.

The pipes for the different inner diameters are summarized in Table 3.3.

Test Section	Material	Number of pieces	length [mm]	outer diameter [mm]	thickness [mm]	inner diameter [mm]	Drilling diameter [mm]	Drilling depth [mm]
ID3	Acryl	3	90	6.0	1.0	3.0	4.0	20.0
	ST35	2	540	4.0	0.5	3.0		
ID5	Acryl	3	90	8.0	1.0	5.0	6.0	20.0
	ST35	2	540	6.0	0.5	5.0		
ID9	Acryl	3	90	16.0	3.0	9.0	10.0	20.0
	ST35	2	540	10.0	0.5	9.0		
ID 14	Acryl	3	90	21.0	3.0	14.0	15.0	20.0
	ST35	2	540	15.0	0.5	14.0		
ID17	Acryl	3	90	26.0	4.0	17.0	18.0	20.0
	ST35	2	540	18.0	0.5	17.0		
ID20	Acryl	3	90	31.0	5.0	20.0	21.0	20.0
	ST35	2	540	21.0	0.5	20.0		
ID25	Acryl	3	90	36.0	5.0	25.0	26.0	20.0
	ST35	2	540	26.0	0.5	25.0		
ID 28	Acryl	3	90	41.0	6.0	28.0	29.0	20.0
	ST35	2	540	29.0	0.5	28.0		

Table 3.3: Summary of pipes

3.5 Scaling of tanks and measurement ranges

In order to scale the size of tanks and range of measurements estimation is made. First assuming a typical test procedure of 10 minutes where ammonia vapor is absorbed into the weak solution. It must be ensured that the amount of weak solution can be distributed and also the rich solution can be stored for further tests or neutralization. Ferreira [8] used a similar single dualpipe with inner diameter of 20.5 mm and his maximum solution and vapor flow rate was 26.2 g/s and 0.48 g/s. Concluding that the maximum flow rates increase linear with the inner diameter respectively with the square meter of the circle the flows are increased by 87%. The corresponding flow rates are 49 g/s and 0.9 g/s. The amount for 10 minutes of testing results in 29.4 kg and 0.54 kg. Regarding to the volume of the test section and pipes and additionally a safety increase for longer testing or the time until steady state is reached the values are doubled resulting in 60 liter volume for the weak and rich solution tank and an ammonia vessel of 1.1 kg. Accordingly the vessels should not be totally filled to ensure compressed air at the top.

3.6 Safety

3.6.1 Anhydrous ammonia

Anhydrous ammonia or ammonia gas (R717) is a colorless gas with a penetrating suffocating odor. Owing to its hygroscopic property ammonia gas is very harmful and can be fatal when inhaling it. A level of just 500 ppm of ammonia in the air is potentially fatal. Owing to the penetrating odor of ammonia gas the perception threshold is 5 ppm. Ammonia dissolves readily in water to give a very corrosive solution and causes serious burns to skin or eyes. It is essential to work in well ventilated areas and care must be taken to avoid any water solubility. Safety glasses and gloves should always be used with ammonia vapor. When eye or skin contact occurred immediately flushing with water is recommended. Furthermore first aid must be called especially when ammonia gas is inhaled.

Ammonia gas can be diluted with air and afterwards ventilated to the environment.

3.6.2 Ammonium hydroxide

Ammonium hydroxide or ammonia solution is a colorless liquid and the boiling point between 38 and 100c depends upon concentration. The solution is extremely damaging to eyes even with dilute solution. Swallowing and contact with skin causes burns due to the previous mentioned hygroscopic property. Therefore glasses with side protection to avoid splashes, gloves and good ventilation is required. Every contact with ammonia solution must immediately be flushed with water and first aid must be called.

Ammonia solution can be diluted with water and afterwards spilled into drain.

3.7 Start and stop procedure

1. Close all valves except V4, V5 and V10.
2. Evacuate via air pump.
3. Close V4, V5 and V10.
4. Open V9 and fill weak Solution Tank with the desired amount.
5. Close V9, start WSP to circulate distilled water through cycle.
6. Start CP to circulate the desired amount of cooling water.
7. Pressurize system via air pump opening V4 and V5.
8. Open V1 and enrich distilled water to desired ammonia concentration.
9. Open V1 to desired amount of ammonia vapor flow and switch 3WV1 to rich solution tank.
10. When steady state is reached start measurement.
11. If further tests with higher concentrated weak solution are desired open V6 to enrich weak and rich solution. Further tests with weak solution can be obtained while mixing solutions with distilled water.
12. Close V1; Switch off coolant flow.
13. Pump weak solution to rich solution tank.
14. Open V6, V7 and use 3WV 2 to exhaust solution to neutralization tank.
15. Depressurize system via shutting down air pump and closing V4 and V5.
16. Spill test rig with distilled water opening V9.

4 Data analysis and reduction

Engineering Equation Solver (EES) together with EES-Refprop interface and the Refprop 8 database is used to calculate the thermo physical properties of ammonia vapor and solution.

4.1 Mass Balance

An overall mass balance is used to verify the mass flow rate of the strong solution corresponding to the coriolis flow meter for the strong solution

$$\dot{m}_{ss} = \dot{m}_{ws} + \dot{m}_{v} . \tag{4.1}$$

The inlet and outlet concentrations are determined with EES from the parameters

$$x = f(T, P, v) . \tag{4.2}$$

The concentration of the strong solution can be verified by using the species mass balance

$$x_{ss} = \frac{\dot{m}_{ws} x_{ws} + \dot{m}_{v}}{\dot{m}_{ss}} \tag{4.3}$$

4.2 Heat transfer

The enthalpies can also be found by using the aforementioned EES

$$h_{s} = f(T_{s}, P_{s}, x_{s}) \tag{4.4}$$

$$h_{v} = f(T_{v}, P_{v}) . \tag{4.5}$$

The heat transfer to the coolant can be calculated with the energy balance on the solution side

$$\dot{Q}_{abs} = \dot{m}_{ws} h_{ws} + \dot{m}_{v} h_{v} - \dot{m}_{rs} h_{rs} \tag{4.6}$$

and compared with the absorber heat load calculated from the coolant side

$$\dot{Q}_{c} = \dot{m}_{c} c_{p} \left(T_{co} - T_{ci} \right) \tag{4.7}$$

to quantify any losses.

The overall heat transfer coefficient U, with the solution as the hot side and coolant as cold side of the absorber is given by

$$U = \frac{q_c}{A \cdot \Delta T_m} \quad , \tag{4.8}$$

where the log-mean temperature difference ΔT_m is determined as

$$\Delta T_m = \frac{\left(T_{ws} - T_{ce}\right) - \left(T_{rs} - T_{ci}\right)}{\ln\left(\frac{T_{ws} - T_{ce}}{T_{rs} - T_{ci}}\right)} \tag{4.9}$$

Note that the absorber analysis used in this study is based on the traditional heat exchanger analysis definition of U.

4.3 Mass transfer

The overall mass transfer coefficient is determined using the vapor flow rate and the heat exchanger surface area

$$H_m = \frac{\dot{m}_v}{\Delta x_{lm} \cdot A} \, , \tag{4.10}$$

where Δx_{lm} denotes the log-mean concentration difference between the solution at the liquid-bubble interface and the bulk solution from the inlet to the exit,

$$\Delta x_{lm} = \frac{\left(x_{ws,sat} - x_{ws}\right) - \left(x_{rs,sat} - x_{rs}\right)}{\ln\left(\frac{x_{ws,sat} - x_{ws}}{x_{rs,sat} - x_{rs}}\right)} \tag{4.11}$$

5 Uncertainty

Uncertainty analysis on all measured variables are performed by the propagation of error proposed by Taylor and Kuyatt [46]

$$W_x = \sqrt{B_x^2 + P_x^2}\,, \tag{5.1}$$

where B_x depicts the systematic (Bias) error and P_x the random uncertainty.

The Bias error B_x for every measured data results from the deviation of each measuring device. Since the test rig is not build and the assignment of the measuring devices has not been decided a typical list of devices with their deviation are listed in Table 5.1 to obtain the Bias error. The Bias error for density measurement can only be obtained from the value of reading and is therefore not listed in the table.

Quantity	Device	Model	Range	Uncertainty	Bias Error
Inlet coolant temperature T_{c1}	Thermocouple	T-Type	−200 to 350 °C	0.3°C	0.3°C
Outlet coolant temperature T_{c2}	Thermocouple	T-Type	−200 to 350 °C	0.3°C	±0.3°C
Coolant mass flow $\dot{m}_c$	Flow meter	FCH-m-POM	0.015 – 1.0 l/min	2%	0.02 l/min
Ammonia vapor temperature T_v	Thermocouple	T-Type	−200 to 350 °C	0.3°C	0.3°C
Ammonia vapor pressure p_v	Pressure transducer	PX482A-200GI	0-13.8 bar	0.3% BFSL	0.0414 bar
Ammonia vapor mass flow $\dot{m}_v$	Flow meter	F-101D/F	2.1 l/min	1.0%	0.021 l/min
Weak solution temperature T_{ws}	Thermocouple	T-Type	−200 to 350 °C	0.3°C	0.3°C
Weak solution density ρ_{ws}	Coriolis flow meter	ACM300		0.5% of reading	
Weak solution pressure p_{ws}	Pressure transducer	PX482A-200GI	0-13.8 bar	0.3% BFSL	0.0414 bar
Weak solution mass flow $\dot{m}_{ws}$	Coriolis flow meter	ACM300	83-5000g/min	0.5% of reading	
Rich solution temperature T_{rs}	Thermocouple	T-Type	−200 to 350 °C	0.3°C	0.3°C
Rich solution density ρ_{rs}	Coriolis flow meter	ACM300		0.5% of reading	

Rich solution pressure p_{rs}	Pressure transducer	PX482A-200GI	0-13.8 bar	0.3% BFSL	0.0414 bar
Rich solution mass flow $\dot{m}_{rs}$	Coriolis flow meter	ACM300	83-5000g/min	0.5% of reading	

Table 5.1: Systematic uncertainty of common measuring devices

The random uncertainty P_x is estimated using the t-distribution. The mean $\bar{x}$ from the n-times measured variable x_i is determined from

$$\bar{x} = \frac{\sum_{i=1}^{n}(x_i)}{n}. \tag{5.2}$$

The standard deviation S_x is calculated from

$$S_x = \sqrt{\sum_{i=1}^{n}\frac{\left(x_i - \bar{x}\right)^2}{(n-1)}}. \tag{5.3}$$

For a given confidence level p the value of the student factor t can be obtained from table 5.2 where the degree of freedom v is calculated from

$$v = n - 1. \tag{5.4}$$

Assuming that the test procedure is running for 10 minutes and the data are collected every 10 seconds the degree of freedom v is 59 and the corresponding student factor t is 2.01 as depicted in Table 5.2.

Degrees of freedom ν	Fraction p in percent					
	68.27[a]	90	95	95.45[a]	99	99.73[a]
1	1.84	6.31	12.71	13.97	63.66	235.80
2	1.32	2.92	4.30	4.53	9.92	19.21
3	1.20	2.35	3.18	3.31	5.84	9.22
4	1.14	2.13	2.78	2.87	4.60	6.62
5	1.11	2.02	2.57	2.65	4.03	5.51
6	1.09	1.94	2.45	2.52	3.71	4.90
7	1.08	1.89	2.36	2.43	3.50	4.53
8	1.07	1.86	2.31	2.37	3.36	4.28
9	1.06	1.83	2.26	2.32	3.25	4.09
10	1.05	1.81	2.23	2.28	3.17	3.96
11	1.05	1.80	2.20	2.25	3.11	3.85
12	1.04	1.78	2.18	2.23	3.05	3.76
13	1.04	1.77	2.16	2.21	3.01	3.69
14	1.04	1.76	2.14	2.20	2.98	3.64
15	1.03	1.75	2.13	2.18	2.95	3.59
16	1.03	1.75	2.12	2.17	2.92	3.54
17	1.03	1.74	2.11	2.16	2.90	3.51
18	1.03	1.73	2.10	2.15	2.88	3.48
19	1.03	1.73	2.09	2.14	2.86	3.45
20	1.03	1.72	2.09	2.13	2.85	3.42
25	1.02	1.71	2.06	2.11	2.79	3.33
30	1.02	1.70	2.04	2.09	2.75	3.27
35	1.01	1.70	2.03	2.07	2.72	3.23
40	1.01	1.68	2.02	2.06	2.70	3.20
45	1.01	1.68	2.01	2.06	2.69	3.18
50	1.01	1.68	2.01	2.05	2.68	3.16
100	1.005	1.660	1.984	2.025	2.626	3.077
∞	1.000	1.645	1.960	2.000	2.576	3.000

Table 5.2: T-distribution for degrees of freedom and confidence level [46]

Therefore the random uncertainty $P_{\bar{x}}$ can be calculated from

$$P_{\bar{x}} = \pm t \frac{S_x}{\sqrt{n}}. \tag{5.5}$$

In order to determine the systematic uncertainty of the calculated results, the systematic uncertainty of each measured variable must be determined. This is done by combining elemental systematic uncertainties by

$$B_R = \sqrt{\sum_{i=1}^{n} \left(B_i \frac{\delta R}{\delta x_i} \right)^2} \tag{5.2}$$

Each partial derivate $\frac{\delta R}{\delta x_i}$ is evaluated by using the average values of the measured variables. When the software EES is used to calculate the enthalpy or concentration of the weak and rich solution the corresponding equation is not known. Therefore the uncertainty of each parameter is accordingly entered into the software and the propagation of error is made by EES which uses the method from Taylor and Kuyatt [46] as described previously.

6 Proposals for further work

From the literature review it can be seen that the influence of a lot of parameters in coupled heat and mass transfer are unknown. The absorber as the “bottleneck” of the absorption system is the most important part to enhance the performance. Therefore several tests have to be made to investigate the heat and mass transfer within the designed bubble absorber. The goal of the experiments is to measure each influencing parameter within the absorber:

- Pressure
- Temperature of coolant, vapor and weak solution
- Mass flow of coolant, vapor and weak solution
- Concentration of weak solution
- Inner diameter of the test section
- Orifice diameter of vapor distribution
- Nozzle geometry of vapor distribution
- Treatment of the inner pipe to induce continual sublaminar boundary layer separation and reattachment [47]
- Bubble flow patterns and there partly heat and mass transfer coefficients
- Surfactants and nano particles to enhance heat and mass transfer

After the collection of measurements a numerical model has to be proposed which describes the coupled heat and mass transfer:

- Bubble growth, disappearance and flow pattern
- Mass transfer in the different bubble flow patterns
- Heat transfer resulting from the mass transfer from the vapor-liquid interface to the bulk solution
- Heat transfer from the bulk solution through the wall to the coolant
- Effect of increasing solution thereby decreasing absorption potential
- Effect of Surfactants and nano particles

When the governing equations are solved and a model to predict heat and mass transfer in a bubble absorber is proposed a sensitivity analysis to find optimum parameters should be considered.

The results would help to design a bubble absorber for a desired amount of heat and mass transfer and the numerical solutions should be experimental proved by a new test rig.

References

[1] Altenkirch, E., Reversible Absorptionsmaschinen, Zeitschrift für die gesamte Kälte-Industrie, 1913

[2] Cardenas, R., *Study of a constrained-film bubble absorber under cycle operating conditions*. 2009.

[3] Cerezo, J., et al., *Experimental study of an ammonia-water bubble absorber using a plate heat exchanger for absorption refrigeration machines.* Applied Thermal Engineering, 2009. **29**(5-6): p. 1005-1011.

[4] Evonik Industries, Produktbeschreibung Plexi-Glas Rohre, 2000

[5] Fan, L.S., et al., *Bubbles in nanofluids.* Industrial & Engineering Chemistry Research, 2007. **46**(12): p. 4341-4346.

[6] Fernández-Seara, J, et al., Ammonia–water absorption in vertical tubular absorbers, International Journal of Thermal Sciences, Volume 44 (3), March 2005, Pages 277-288.

[7] Fernández-Seara, J., F.J. Uhía, and J. Sieres, *Analysis of an air cooled ammonia-water vertical tubular absorber.* International Journal of Thermal Sciences, 2007. **46**(1): p. 93-103.

[8] Ferreira, C.A.I., C. Keizer, and C.H.M. Machielsen, *Heat and mass transfer in vertical tubular bubble absorbers for ammonia-water absorption refrigeration systems.* International Journal of Refrigeration, 1984. **7**(6): p. 348-357.

[9] Ferreira, C.A., *Combined momentum, heat and mass transfer in vertical slug flow absorbers.* International Journal of Refrigeration, 1985. **8**(6): p. 326-334.

[10] Garimella, S. *Miniaturized Heat and Mass Transfer Technology for Absorption Heat Pumps*. in *Proceedings of the International Sorption Heat Pump Conference*. 1999. Munich, Germany.

[11] Garimella, S., *Method and means for miniaturization of binary-fluid heat ans mass exchangers*, in *United States Patent*. 2004. **US6802364B1.**

[12] Goel, N. and D.Y. Goswami, *A Compact Falling Film Absorber.* Journal of Heat Transfer, 2005. **127**(9): p. 957-965.

[13] Goel, N. and D.Y. Goswami, *Experimental Verification of a New Heat and Mass Transfer Enhancement Concept in a Microchannel Falling Film Absorber.* Journal of Heat Transfer, 2007. **129**(2): p. 154-161.

[14] Higbie, R., *The rate of absorption of a pure gas into a still liquid during short period exposure.* Trans Am Inst Chem Engng, 1935. **31**: p. 356-389.

[15] Horn, R.K., *Messungen zum Wärme und Stoffübergang am Rieselfilm.* Thesis Univ. Karlsruhe, 1970.

[16] Hozawa, M., et al., *Marangoni Convection during Steam Absorption into Aqueous Libr Solution with Surfactant.* Journal of Chemical Engineering of Japan, 1991. **24**(2): p. 209-214.

[17] Jenks, J., *An Experimental Study of Ammonia-Water Bubble Absorption in a Constrained Microscale Film*. 2007, Oregon State University.

[18] Kang, Y.T., R.N. Christensen, and T. Kashiwagi, *Ammonia-Water Bubble Absorber with a Plate Heat Exchanger.* ASHRAE Transactions, 1998. **Vol. 104**(1).

[19] Kang, Y.T., A. Akisawa, and T. Kashiwagi, *Experimental correlation of combined heat and mass transfer for NH3-H2O falling film absorptionCorrélation expérimentale entre le transfert de chaleur et de masse pour de l'absorption au NH3-H2O à film tombant.* International Journal of Refrigeration, 1999. **22**(4): p. 250-262.

[20] Kang, Y.T., A. Akisawa, and T. Kashiwagi, *Visualization and model development of Marangoni convection in NH3-H2O systemVisualization et développement d'un modèle de convection de Marangoni dans un système à NH3-H2O.* International Journal of Refrigeration, 1999. **22**(8): p. 640-649.

[21] Kang, T.Y., A. Akisawa, and T. Kashiwagi, *Analytical investigation of two different absorption modes: falling film and bubble types.* International Journal of Refrigeration, 2000. **23**(6): p. 430-443.

[22] Kang, Y.T., T. Nagano, and T. Kashiwagi, *Visualization of bubble behavior and bubble diameter correlation for NH3-H2O bubble absorption.* International Journal of Refrigeration, 2002. **25**(1): p. 127-135.

[23] Kang, Y.T. and T. Kashiwagi, *Heat transfer enhancement by Marangoni convection in the NH3-H2O absorption process.* International Journal of Refrigeration-Revue Internationale Du Froid, 2002. **25**(6): p. 780-788.

[24] Kang, T.Y., T. Nagano, and T. Kashiwagi, *Mass transfer correlation of NH3-H2O bubble absorption.* International Journal of Refrigeration, 2002. **25**(7): p. 878-886.

[25] Kars, R.L., R.J. Best, and A.A.H. Drinkenburg, *Sorption of Propane in Slurries of Active-Carbon in Water.* Chemical Engineering Journal and the Biochemical Engineering Journal, 1979. **17**(3): p. 201-210.

[26] Kashiwagi, T., *Basic mechanism of absorption heat and mass transfer enhancement by the Marangoni effect.* Newsletter, IEA Heat Pump Center, 1988. **6**(4): p. 2-6.

[27] Killion, J.D. and S. Garimella, *A critical review of models of coupled heat and mass transfer in falling-film absorption.* International Journal of Refrigeration, 2001. **24**(8): p. 755-797.

[28] Kim, H.Y., B.B. Saha, and S. Koyama, *Development of a slug flow absorber working with ammonia-water mixture: part I - flow characterization, and experimental investigation.* International Journal of Refrigeration-Revue Internationale Du Froid, 2003. **26**(5): p. 508-515.

[29] Kim, H.Y., B.B. Saha, and S. Koyama, *Development of a slug flow absorber working with ammonia-water mixture: part II - data reduction model for local heat and mass transfer characterization.* International Journal of Refrigeration-Revue Internationale Du Froid, 2003. **26**(6): p. 698-706.

[30] Kim, J.K., et al., *The effect of chemical surfactants on the absorption performance during NH3/H2O bubble absorption process.* International Journal of Refrigeration-Revue Internationale Du Froid, 2006. **29**(2): p. 170-177.

[31] Kim, J.K., J.Y. Jung, and Y.T. Kang, *The effect of nano-particles on the bubble absorption performance in a binary nanofluid.* International Journal of Refrigeration-Revue Internationale Du Froid, 2006. **29**(1): p. 22-29.

[32] Kim, J.K., J.Y. Jung, and Y.T. Kang, *Absorption performance enhancement by nano-particles and chemical surfactants in binary nanofluids.* International Journal of Refrigeration-Revue Internationale Du Froid, 2007. **30**(1): p. 50-57.

[33] Krishnamurthy, S., et al., *Enhanced mass transport in nanofluids.* Nano Letters, 2006. **6**(3): p. 419-423.

[34] Kwon, K. and S. Jeong, *Effect of vapor flow on the falling-film heat and mass transfer of the ammonia/water absorber.* International Journal of Refrigeration, 2004. **27**(8): p. 955-964.

[35] Lee, K.B., et al., *Experimental analysis of bubble mode in a plate-type absorber.* Chemical Engineering Science, 2002. **57**(11): p. 1923-1929.

[36] Ma, X.H., et al., *Enhancement of bubble absorption process using a CNTs-ammonia binary nanofluid.* International Communications in Heat and Mass Transfer, 2009. **36**(7): p. 657-660.

[37] Meacham, J.M. and S. Garimella. *Experimental Demonstration of a Prototype Microchannel Absorber for Space-Conditioning Systems*. in *International Sorption Heat Pump Conference*. 2002. Shanghai, China.

[38] Meacham, J.M. and S. Garimella, *Modeling of Local Measured Heat and Mass Transfer Variations in a Microchannel Ammonia-Water Absorber.* ASHRAE Transactions, 2003. **109**(1): p. 412-422.

[39] Meacham, J.M. and S. Garimella, *Ammonia-Water Absorption Heat and Mass Transfer in Microchannel Absorbers with Visual Confirmation.* ASHRAE Transactions, 2004. **Vol. 110**(1): p. 525-532.

[40] Merrill, T.L., Setoguchi, T., and Perez-Blanco H., Compact bubble absorber design and analysis, *ASME International Absorption Heat Pump Conference*, AES-Vol. 31, pp. 217-223, (1994).

[41] Merrill, T.L., T. Setoguchi, and H. Perezblanco, *Passive Heat-Transfer Enhancement Techniques Applied to Compact Bubble Absorber Design.* Journal of Enhanced Heat Transfer, 1995. **2**(3): p. 199-208.

[42] Moller, R. and K.F. Knoche, *Surfactants with NH3-H2O.* International Journal of Refrigeration-Revue Internationale Du Froid, 1996. **19**(5): p. 317-321.

[43] Niebergall, W., *Handbuch der Kältetechnik: Sorptions-Kätemaschinen 7. Band*. 1959: Springer-Verlag GmbH

[44] Perez-Blanco, H., *A model of an ammonia-water falling film absorber.* ASHRAE Transactions, 1988. **94**(1): p. 467–483.

[45] Summerheat Leitfaden

[46] Taylor, B.N. and C.E. Kuyatt, *Guidelines for evaluating and expressing the uncertainty of NIST measurement results.* NIST Technical Note, 1994. **1297**

[47] Webb, R.L., E.R.G. Eckert, and Goldstei.Rj, *Heat Transfer and Friction in Tubes with Repeated-Rib Roughness.* International Journal of Heat and Mass Transfer, 1971. **14**(4): p. 601-&.